BIOCHEMISTRY

 Volume 45, Number 27 July 11, 2006

Articles

Biochemical and Structural Studies of N^5-Carboxyaminoimidazole Ribonucleotide Mutase from the Acidophilic Bacterium *Acetobacter aceti*†

Charles Z. Constantine, Courtney M. Starks, Christopher P. Mill, Aaron E. Ransome, Steven J. Karpowicz, Julie A. Francois, Rena A. Goodman, and T. Joseph Kappock*

Department of Chemistry, Washington University, St. Louis, Missouri 63130-4899

Received March 8, 2006; Revised Manuscript Received May 5, 2006

ABSTRACT: N^5-Carboxyaminoimidazole ribonucleotide (N^5-CAIR) mutase (PurE) catalyzes the reversible interconversion of acid-labile compounds N^5-CAIR and 4-carboxy-5-aminoimidazole ribonucleotide (CAIR). We have examined PurE from the acidophilic bacterium *Acetobacter aceti* (*Aa*PurE), focusing on its adaptation to acid pH and the roles of conserved residues His59 and His89. Both *Aa*PurE and *Escherichia coli* PurE showed quasi-reversible acid-mediated inactivation, but wt *Aa*PurE was much more stable at pH 3.5, with a ≥20 °C higher thermal unfolding temperature at all pHs. His89 is not essential and does not function as part of a proton relay system. The k_{cat} pH−rate profile was consistent with the assignment of pK_1 to unproductive protonation of bound nucleotide and pK_2 to deprotonation of His59. A 1.85 Å resolution crystal structure of the inactive mutant H59N-*Aa*PurE soaked in CAIR showed that protonation of CAIR C4 can occur in the absence of His59. The resulting species, modeled as isoCAIR [4(*R*)-carboxy-5-iminoimidazoline ribonucleotide], is strongly stabilized by extensive interactions with the enzyme and a water molecule. The carboxylate moiety is positioned in a small pocket proposed to facilitate nucleotide decarboxylation in the forward direction (N^5-CAIR → CAIR) [Meyer, E., Kappock, T. J., Osuji, C., and Stubbe, J. (1999) *Biochemistry 38*, 3012−3018]. Comparisons with model studies suggest that in the reverse (nonbiosynthetic) direction PurE favors protonation of CAIR C4. We suggest that the essential role of protonated His59 is to lower the barrier to decarboxylation by stabilizing a CO_2−azaenolate intermediate.

The fifth metabolite of de novo purine biosynthesis (*1*), 5-aminoimidazole ribonucleotide (AIR),[1] is carboxylated by at least two biosynthetic routes that involve different forms of PurE, designated as N^5-carboxyaminoimidazole ribonucleotide (N^5-CAIR) mutase (class I, EC 5.4.99.18) or AIR carboxylase (class II, EC 4.1.1.21) (*2*). The first route is found in bacteria, yeasts, and plants, where AIR, ATP, and bicarbonate are converted to N^5-CAIR, ADP, and inorganic phosphate (P_i) by N^5-CAIR synthetase (PurK, EC 6.3.4.18)

† This research was supported by Grant 531-HF02 from the Herman Frasch Foundation and Career Award MCB 0347250 from the National Science Foundation to T.J.K. C.Z.C. was partly supported by Graduate Assistance in Areas of National Need (GAANN) Grant 200A010213 from the Department of Education. Mass spectrometry was provided by the Washington University Mass Spectrometry Resource, supported by the NIH (P41RR0954).

* To whom correspondence should be addressed: kappock@wustl.edu (e-mail); 314-935-8241 (phone); 314-935-4481 (fax).

[1] Abbreviations: AIR, 5-aminoimidazole ribonucleotide; N^5-CAIR, N^5-carboxyaminoimidazole ribonucleotide; CAIR, 4-carboxy-5-aminoimidazole ribonucleotide; PRA, phosphoribosylamine; spp., species; *Aa*PurE, PurE from *Acetobacter aceti*; *Ec*PurE, PurE from *Escherichia coli*; wt, wild type; FF, fast flow; ODN, oligodeoxynucleotide; UTR, untranslated region; AS, ammonium sulfate; CD, circular dichroism; isoCAIR, 4(*R*)-carboxy-5-iminoimidazoline ribonucleotide; NAIR, 4-nitro-5-aminoimidazole ribonucleotide.

10.1021/bi060465n CCC: $33.50
Published on Web 06/16/2006

Scheme 1

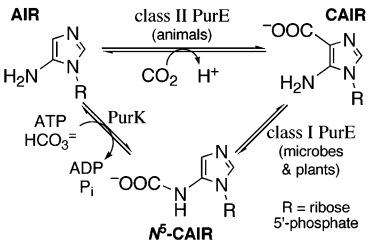

(*3*, *4*). N^5-CAIR is then converted to 4-carboxy-5-aminoimidazole ribonucleotide (CAIR) by a class I PurE in an apparently intramolecular, multistep rearrangement (Scheme 1) (*5*). Class I PurEs are either individual proteins or C-terminal fusions to PurK domains (*3*). The second route is found in animals, where a class II PurE appears to convert AIR and CO_2 directly to CAIR, without need for PurK (*6*). Even though they act on different substrates, the two PurE classes have similar sequences and are thought to perform similar enzyme chemistry (*3*, *5*). While the participation of N^5-CAIR in class II systems has not been definitively ruled out, all completely sequenced animal genomes lack recognizable PurK genes, and the two PurE classes have distinct, strictly conserved regions (*2*). The euryarchaeote *Archaeoglobus fulgidus* contains a class II PurE, which may correlate with available environmental CO_2 (*5*). All other class II PurEs are C-terminal fusions to 4-(*N*-succinocarboxamide)-5-aminoimidazole ribonucleotide synthetase (PurC, EC 6.3.2.6) domains (*3*). Other PurE types, such as the PurE−PurE′ internal duplication found in methanogenic Archaea, may be additional biosynthetic variants (*2*).

Biochemical analysis of PurE is complicated by the temperature- and pH-dependent interconversions of bicarbonate/CO_2 and AIR with carboxylated nucleotides. N^5-CAIR decomposes rapidly to AIR and CO_2 at acid pH; N^5-CAIR forms in AIR solutions containing millimolar bicarbonate/CO_2. This lability hindered the identification of N^5-CAIR as the true substrate for class I PurE (*3*).

In the PurK−PurE carboxylase system, AIR functions as a CO_2 carrier comparable to the biotin cofactors present in multiprotein carboxylases (*3*). PurK and biotin carboxylase are structurally similar ATP-grasp enzymes (*7*, *8*) that are thought to use carboxyphosphate as a transient intermediate in the formation of N^5-CAIR or *N*-carboxybiotin (*3*, *9*, *10*). The chemical lability of the two N-carboxylated carriers could pose a challenge to efficient metabolic flux. Restricted diffusion might improve transfer efficiency: while there is at present no evidence that requires it, N^5-CAIR might be channeled from PurK to PurE, just as biotin is tethered to multienzyme complexes.

N^5-CAIR lability would be a particular problem in thermophiles or acidophiles that tolerate acidic cytoplasmic pH. *Acetobacter aceti* is an example of the latter. *A. aceti* creates a highly acidic environment by converting ethanol to acetic acid and is used to make vinegar (*11*). The membrane-permeable acetic acid leaks into nonresistant organisms, poisoning them and deenergizing them by collapsing the proton gradient. To maintain a normal proton gradient, *A. aceti* allows cytoplasmic pH to drop (to as low as pH 4) in register with external pH (*12*).

Cytoplasmic acidification would accelerate the decomposition of the two particularly acid-labile purine biosynthetic intermediates, phosphoribosylamine (PRA, the product of the first committed pathway step) and N^5-CAIR. This may pose a problem for efficient purine biosynthesis in *A. aceti* (*13*), which is generally grown at 30 °C. Published decomposition rates can be extrapolated to estimate half-lives of 0.23 s for PRA and 0.07 s for N^5-CAIR at pH 4 and 30 °C (*3*, *14*). To understand this aspect of *A. aceti* metabolism, we have studied its PurE. While the sequences of *A. aceti* PurE (*Aa*PurE) and *Escherichia coli* PurE (*Ec*PurE) are 52% identical, their crystal structures reveal many surface differences that may be relevant to the adaptation of *Aa*PurE for acidic conditions (*2*, *13*). The PurEs from *A. aceti* (a mesophilic acidophile) and *Thermotoga maritima* (a thermophilic neutralophile) resemble each other more than the PurE from *E. coli* (a mesophilic neutralophile), suggesting that *Aa*PurE might be a thermostable protein (*13*).

We report here the cloning, purification, and biochemical and biophysical studies of wild-type (wt) *Aa*PurE and mutants lacking one of two conserved His residues. Structures of wt and mutant *Aa*PurEs, some in complex with nucleotides, support and extend a previously proposed mechanism for *Ec*PurE (*5*) and define the function of *Aa*PurE His59 (*Ec*PurE His45).

EXPERIMENTAL PROCEDURES

Materials and Methods. Unless otherwise noted, all chemicals and enzymes were obtained from Sigma or Fisher in the highest purity available. DNA-modifying enzymes and Vent DNA polymerase were from New England Biolabs. Kits for λBlueStar phage library construction and packaging were obtained from Promega. Biotinylated probes were detected using a North2South chemiluminescent kit from Pierce. Routine DNA isolations were performed using Qiagen kits. DEAE-Sepharose Fast Flow (FF), iminodiacetic acid Sepharose 6B FF, Sephadex G25 (medium), and QAE-cellulose FF were purchased from Amersham or Sigma. Hydroxyapatite HTP was from Bio-Rad. H. Jiang and K. LeChevet of this laboratory synthesized CAIR ribonucleoside, CAIR, and AIR from 5-aminoimidazole-4-carboxamide ribonucleoside (Toronto Research Chemicals) as described (*15*, *16*). A VirSonic 100 sonicator was used for cell disruption. Centrifugation steps were performed in a Beckman Avanti J-20 centrifuge with JLA-10.5 or JA-20 rotors. Protein ultrafiltration was performed using either YM10 or PM30 membranes in an Amicon pressure cell. Protein concentrations were determined using a Bio-Rad Bradford kit with bovine serum albumin (BSA) as standard. N-Terminal sequencing by Edman degradation was performed by Midwest Analytical, Inc., using purified protein.

Bacterial Strains. *E. coli* strain PC0135 [CGSC 5403, *lacY1 purE55 glnV44(AS) gal-3 rpsL117(str^R) malT1(Lam^R) xylA7 mtlA2 thi-1*] was obtained from the *E. coli* Genetic Stock Center at Yale University (*17*). *E. coli* strain BM25.8 [*(F′ traD36 lacI^q lacZΔM15 proA$^+$B$^+$) supE thi* Δ*(lac-proAB) P1 Cm^R hsd^R (r$_{K12}^-$ m$_{K12}^+$) (λimm^{434}Kan^R)*] was from Novagen. Routine cloning and mutagenesis steps were performed using *E. coli* strains DH5α or XL10Gold. *A. aceti* 1023 was the generous gift of Dr. Etsuko Etani (Mitsukan Corp., Aichi, Japan).

Genomic DNA (gDNA) Isolation and Purification. A literature method (*62*) was adapted for use with *A. aceti* 1023,

which was maintained at 35 °C in YPD media supplemented with 2% (v/v) ethanol. Liquid cultures (1 L) in 2.8 L Fernbach shaker flasks were inoculated from glycerol stocks and grown for 24 h at 35 °C with agitation at 220 rpm in an incubator shaker (New Brunswick Scientific C25). Cells (about 4 g/L of culture) were harvested by centrifugation (3080*g*, 25 min), washed once in water (10 mL/g of cells), washed twice in 1 M NaCl (10 mL/g and then 2.5 mL/g of cells), and resuspended in TE (10 mM Tris·HCl, pH 8.0, 1 mM EDTA; 1.3 mL/g of cells) in one 50 mL conical tube per liter of culture. Steps 3−7 of the published protocol were then performed as described but at a much larger scale, resulting in a pellet that was resuspended in TE (15 mL) and allowed to redissolve at 55 °C for 18 h. The solution was adjusted to 2 μg/mL with RNase A, then placed in a dialysis bag (12−14 kDa cutoff), and dialyzed against TE (1 L) for 18 h at room temperature. gDNA solutions were stored for up to 1 week at 4 °C.

Characterization of the PC0135 purE Mutation. PC0135 gDNA was isolated using DNAzol (Molecular Research Center) and used as a PCR template. A 2 kbp PCR product containing the entire *E. coli purE*−*purK* region was obtained with Vent DNA polymerase and oligodeoxynucleotides (ODNs) 1161 and 1162 as primers (ODN sequences are given in Table S1 in Supporting Information). The sequence of the PCR product was obtained from both strands using terminal and internal primers.

Cloning of A. aceti purE−*purK*. *A. aceti* gDNA (0.4 μg) was limit-digested with *Sph*I (mostly 1−4 kb fragments), ligated into the *Sph*I site in pUC118, and transformed into PC0135 cells, which were grown on M9 minimal media supplemented with 100 μg/mL ampicillin. Plasmid pJK173 was isolated from a colony that appeared after 72 h at 37 °C. DNA sequences obtained by walking with vector- and gene-specific primers were assembled into a 2073 bp contig using the Staden package (*18*). Open reading frames (ORFs) were identified using sequence comparisons and the FGENESB program (Softberry).

Phage Library Construction and Screening. A Qiagen 500/G genomic tip was used to further purify gDNA after dialysis against TE. gDNA digested for 30 min at 37 °C with *Sau*3AI (2.5 units, at 1.3 units/mL) was separated using a 20−40% sucrose gradient for 24 h at 10 °C (111000*g*). Fractions containing ∼15 kb DNA fragments were used to build a λBlueStar phage library (2×10^6 pfu/mL) following the manufacturer's instructions. Plaque lifts onto PVDF membranes (0.22 μm, Millipore) were probed with *Aa*PurE-specific 5′-biotinylated ODN 686 and chemiluminescent detection. Eight positive plaques were converted to plasmids in strain BM25.8 and tested by PCR for the presence of the internal *purE* sequence. Positive clone pJK193 was sequenced by primer walking, and a 6842 bp portion of the insert sequence was assembled using the Staden package.

Construction of PurE and PurK Expressers. A PCR product spanning the *purE*−*purK* region was obtained using Vent DNA polymerase, plasmid pJK173 as template, and ODNs 408 and 614 as primers that introduce flanking 3′ *Eco*RI and 5′ *Nde*I sites, respectively. ODN 614 also converted the *purE* GTG start codon into an ATG. The PCR product was cloned into pET23a to yield plasmid pJK174, used for coexpression of *Aa*PurE and *Aa*PurK. A PCR product obtained with ODNs 614 and 615 was cloned into pET23a to yield plasmid pJK175, used for expression of PurE only. In pJK174 and pJK175, *Aa*PurE is produced with an additional N-terminal Met residue. The *purK* gene was amplified by PCR with ODNs 408 and 410 and cloned into pET28a to yield plasmid pJK130. In pJK130, PurK is produced with a 20 amino acid N-terminal extension containing a hexahistidine sequence (H6*Aa*PurK). Mutagenesis was performed using the QuikChange kit (Stratagene) with complementary ODN pairs. All plasmids contained the expected DNA sequences.

Construction of Plasmids for Functional Complementation Studies. QuikChange mutagenesis of the *purE* region in pJK173 [*purE*−*purK*, with a 318 bp 5′ untranslated region (UTR) and 36 bp 3′ UTR] was used to create plasmids pJK347 (H59D-*Aa*PurE/*Aa*PurK) and pJK348 (H59N-*Aa*PurE/*Aa*PurK). The *purE* region, flanked by a 39 bp 5′-UTR and 14 bp 3′-UTR, was PCR amplified (ODNs 1078 and 1079 primers) and cloned into pUC118, using *Eco*RI and *Hin*dIII sites added by the PCR primers, to generate plasmid pJK324. QuikChange mutagenesis of pJK324 was used to create pJK340 (H59N-*Aa*PurE) and pJK346 (H59D-*Aa*PurE). In pJK173 and pJK324 plasmids, *purE* is in the same orientation with respect to the *lac* promoter in pUC118. The smaller 5′-UTR in pJK324 contains the 43 bp region between the *E. coli lpxH* and *purE* genes, which was assumed to harbor upstream elements needed to express the *purE*−*purK* operon.

Functional Complementation Studies. Plasmids described in the preceding section were transformed into PC0135 and assessed for their ability to restore prototrophy (pur^+) on solid minimal medium (*19*) supplemented with 10 μM thiamin and 100 μg/mL carbenicillin. Cells were grown at 37 °C. A single colony of each strain was used to inoculate a small LB/Amp culture. After overnight growth, a portion of the culture was diluted in LB to give a final $A_{600} = 0.0004$. An aliquot (50 μL) of the resulting dilution was spread on solid media as described above. Some plates were supplemented with hypoxanthine (15 μg/mL) to supply purines. For all plasmids except pJK347, a set of plates were also placed in a CO_2-enriched atmosphere ("candle jar") as described (*4*).

Isolation of PurE. BL21(DE3) cells transformed with pJK174 or pJK175 were grown to saturation at 37 °C in LB supplemented with 0.1 mg/mL ampicillin. After a 1:50 dilution into fresh medium, cells were grown at 37 °C to $A_{600} = 0.6$. IPTG was then added to 0.4 mM, and growth was continued another 4 h. All subsequent steps were performed at 4 °C. Cells (4 g/L of culture) were harvested by centrifugation (10000*g*, 20 min), resuspended in 50 mM Tris·HCl, pH 8.0 (6 mL/g of cells), and disrupted by sonication (three cycles of 30 s). Debris was removed by centrifugation at 37000*g* for 20 min. The supernatant was adjusted to 1% streptomycin from a 10% (w/v) stock and stirred another 15 min. Solids were removed by centrifugation (37000*g*, 60 min), and the supernatant was adjusted to 35% saturation by the addition of solid ammonium sulfate (AS) over 30 min. After another 30 min stirring, solids were collected by centrifugation (37000*g*, 10 min). The supernatant contained nearly all of the PurK activity (data not shown). The pellet containing PurE was redissolved in a minimal volume of 10 mM potassium phosphate, pH 8.0, and applied in 2.5 mL portions to a PD10 column (1.5 × 5 cm) equilibrated in the same buffer. Desalted protein fractions were applied to a hydroxyapatite column (2.5 × 1.5 cm)

equilibrated in the same buffer. The column was washed with 10 mM potassium phosphate, pH 8.0 (4 column volumes). Fractions containing *Aa*PurE, which does not adsorb to hydroxyapatite, were pooled and concentrated to >5 mg/mL with an UltraFree-MC (Amicon) ultrafiltration device containing a YM10 membrane. The protein solution was frozen in small, single-use aliquots and stored at −80 °C.

*Aa*PurE mutants were isolated using the wt procedure from BL21(DE3) cells transformed with pJK283 (H59N), pJK282 (H59D), pJK281 (H59F), pJK318 (H59Q), pJK319 (H59A), pJK320 (H59S), pJK278 (H89N), pJK279 (H89D), pJK280 (H89F), pJK314 (H89V), or pJK315 (H89G). To eliminate any risk of cross-contamination, each mutant protein was prepared using its own columns and ultrafiltration devices.

Enzyme Activity Assays. PurE was assayed using published methods (*3*, *4*). Specific activities for PurE were determined in the reverse direction (CAIR → N^5-CAIR) at 30 °C in a stoppered, masked, 1 cm path length cuvette containing 50 mM Tris·HCl, pH 8.0, 0.1 mM CAIR, and 0.057 μg of wt *Aa*PurE (6 nM [subunits]), in a final volume of 0.5 mL. Reactions were initiated by the addition of PurE, and initial rates (<10% conversion of CAIR) were determined at 260 nm ($\Delta\epsilon_{260}$ = 8.93 mM^{-1} cm^{-1}) (*4*), after a correction for the small background rate. A 0.5 cm path length cuvette was used for activity assays at high [CAIR]. Kinetic constants were obtained by nonlinear least-squares fitting to the Michaelis−Menten equation using Kaleidagraph 3.6 (Synergy Software). A unit is defined as the formation of 1 μmol of product/min.

pH−Rate Profiles. The decomposition of CAIR is monitored by a decrease at 260 nm, a wavelength for which the extinction coefficients of AIR and N^5-CAIR are similar (*3*, *4*). This assay is therefore insensitive to subsequent decarboxylation of N^5-CAIR to AIR, which occurs at significant rates that increase at low pH ($t_{1/2}$ = 0.9 min^{-1} at 37 °C and pH 7.8) (*3*). To construct a pH−rate profile for PurE, $\Delta\epsilon_{260}$ values were first determined with a standardized CAIR solution using end point assays at many pH values (Supporting Information) (*4*). These values compared well to $\Delta\epsilon_{260}$ values computed from known extinction coefficients for AIR and CAIR at pH 6, 7, and 8 (Figure S2 in Supporting Information). Rates were determined as described above, except that a three-buffer system was employed to fix pH at a constant ionic strength of 0.1 M (*20*). Each reaction (final volume 0.5 mL) contained 100 mM Tris·HCl, 50 mM MES, 50 mM acetic acid, variable [CAIR] (0.4−400 μM), and either 0.54−4.3 nM wt *Aa*PurE or 36.5−365 nM H59D-*Aa*PurE. Nonlinear least-squares fits of y (either k_{cat} or k_{cat}/K_m, obtained from fits to the Michaelis−Menten equation) to eq 1 yielded c, the pH-independent form of the parameter y and K values. In one case, an expression that accounts for three ionizations, two of which (K_1) are indistinguishable, was used to fit the data (eq 2).

$$\log y = \log\left[\frac{c}{1 + H/K_1 + K_2/H}\right] \quad (1)$$

$$\log y = \log\left[\frac{c}{1 + (H/K_1)^2 + K_2/H}\right] \quad (2)$$

Maximal Activities for Inactive AaPurE Mutants. Standard activity assays were altered to contain up to 0.9 mg/mL protein to detect any residual activity. For H59N-*Aa*PurE this procedure was also performed using the three-buffer system at pH 5.0, 6.0, 7.0, and 8.0 with either 0.2 or 0.8 mg/mL mutant PurE in the activity assay. The maximum possible residual enzyme activity was taken to be the uncertainty in the slope of A_{260} versus time.

Fluorescence Titrations. Spectra were obtained with a Spex FluoroMax equipped with a thermostated stirred cell holder at 25 °C using a 1 cm fluorometer cell that contained 2.0 mL prior to the titration. The excitation wavelength was 295 nm (1 nm slit width), and emission spectra were collected from 300 to 420 nm (5 nm slit width, 0.5−0.75 s integration every nanometer). The intensity of the fluorescence emission F for each titration point was measured at the emission λ_{max} and then corrected for dilution and inner filter effects.

Citrate titrations were performed in 50 mM potassium acetate, pH 5.2, 100 mM KCl, and 3 μM *Aa*PurE [subunit], using 100 mM potassium citrate as titrant. Citrate titration data F were fit as a function of C = [titrant] to three parameters (eq 3): K_d = dissociation constant, $F_o = F$ at zero titrant, and ΔF = maximal change in F.

$$F = F_o - \Delta F\frac{C}{C + K_d} \quad (3)$$

CAIR titrations were performed in 50 mM Tris·HCl, pH 8.0, using 3 μM *Aa*PurE, with 100 mM CAIR in 50 mM Tris as the titrant. Immediately prior to each titration, CAIR stock solutions were standardized by end point assays, with 3.5 nmol (2.5 units) of wt *Aa*PurE used to initiate rapid conversion to product at pH 8. CAIR titration data were fit, using known values of C and E = 0.5[subunit], to the same three parameters (eq 4). Half-sites binding was selected because there is no evidence for simultaneous occupancy of more than four active sites in the octamer by nucleotides and it yields superior fits to the titration data.

$$F = F_o - \frac{\Delta F}{2}[(C + E + K) - \sqrt{(C + E + K)^2 - 4EC}] \quad (4)$$

Citrate pH−Affinity Profile. Individual citrate titrations performed using wt *Aa*PurE at pH 3.5−6.4 in 50 mM potassium acetate and 100 mM KCl, at 3 μM *Aa*PurE, yielded K_a values that were fit to eq 5. This expression accounts for the fraction of citrate that forms a dianion in solution. For some fits, the known citrate pK (pK_2 = 4.76) (*21*) was allowed to vary.

$$K_a = \frac{K_a^{max}}{\left[\left(\frac{10^{-pH}}{10^{-pK_1}}\right)\left(\frac{10^{-pH}}{10^{-4.76}}\right) + \left(\frac{10^{-pK_2}}{10^{-pH}}\right) + 1\right]} \quad (5)$$

Solution Studies. Analytical gel filtration was performed using a Tosoh-Biosep TSK-Gel G2000SWXL column attached to a Waters Breeze HPLC or Amersham Akta system. The mobile phase was 50 mM sodium phosphate buffer with 0.15 M KCl at pH 6.8, applied at 0.5 mL/min. Injections (20 μL) contained 0.4 mg of protein. Gel filtration size standards (670−1.3 kDa; Bio-Rad) were used to determine protein solution sizes.

Circular Dichroism (CD). CD data were obtained on a Jasco J-500A spectropolarimeter. Spectra were corrected by subtracting a buffer-only background. A jacketed cylindrical quartz cell with a 0.1 cm optical path length was heated from 24 to >85 °C in 1 or 2 °C steps, allowing 150 s for equilibration at each temperature (within a ±0.3 °C instrumental deadband). Temperature-induced changes in the structure of *Aa*PurE or *Ec*PurE (0.23 mg/mL in 50 mM potassium phosphate and 100 mM KCl at various pHs) were monitored by measuring the ellipticity at 222 nm. Sample chamber temperatures are given, which were derived from observed values using a cell-specific calibration curve. The steepest part of each progress curve was taken as the melting temperature (T_m).

Acid Stability Assays. PurE was incubated at 30 μg/mL (1.6 nM) in the three-buffer system (see pH−Rate Profiles above) at 30 °C and pH 3.0 or 3.5. Aliquots were withdrawn and immediately added to prepared reverse-direction activity assays at 30 °C. Experiments were also performed in 25 mM potassium phosphate, pH 2.5, with KCl added to a final ionic strength of 0.1 M.

Crystallization and Soaking of AaPurE Forms. *Aa*PurE forms intended for crystal production were applied to a Superdex 200 column equilibrated in and developed with 20 mM Tris·HCl, pH 8.0, and 50 mM NaCl. Fractions containing protein were diluted in 5−10 mM Tris·HCl, pH 8, and 15−50 mM NaCl and then concentrated to 15−20 mg/mL using an Amicon Ultra concentrator (MWCO 30000). Crystals were grown by the hanging drop vapor diffusion method using reservoir solutions at low pH [21−23% (w/v) PEG 4000, 190 mM ammonium acetate, 90 mM sodium citrate, pH 5.4] or at high pH (28−30% PEG 4000, 200 mM $LiSO_4$, 100 mM Tris·HCl, pH 8−8.5). To generate nucleotide-bound complexes, crystals were soaked for 1−3 h in artificial mother liquor containing 0.1−0.5 mM CAIR. For data collection at pH 7 in the absence of sulfate, high pH grown crystals of wt *Aa*PurE, H59D-*Aa*PurE, and H89N-*Aa*PurE were soaked for 1−3 h in 30% PEG 4000, 200 mM LiCl, 100 mM HEPES, pH 7, and 0.1−0.2 mM CAIR.

X-ray Data Collection and Processing. Prior to data collection, crystals were placed briefly into a cryoprotectant solution that consisted of artificial mother liquor with an additional 2% PEG 4000 and 15% (v/v) ethylene glycol. Crystals were then frozen in a nitrogen gas stream at 111 K, and data were collected on a Rigaku R-Axis IV image plate detector using a graphite-monochromated Cu Kα X-ray beam from a Rigaku RU200 generator operated at 5 keV. Diffraction data were indexed, integrated, and scaled with HKL2000.

Structure Determination and Refinement. All crystals had the same unit cell and space group observed previously (PDB code 1u11) (*13*). Structures were determined by placing the 1u11 model into each unit cell using rigid-body refinement. Models were then refined using simulated annealing, positional refinement, individual *B*-factor refinement, and water picking in CNS (*22*) and manual inspection and rebuilding in O (*23*). Starting coordinates for bound ions and nucleotides were obtained from the HIC-UP server (*24*), and CNS topology and parameter files were generated by the PRODRG server (*25*). The H59D-*Aa*PurE·AIR complex was further refined using REFMAC (*26*, *27*). Coordinates and structure factors have been deposited in the RCSB Protein Data Bank (PDB) with accession numbers 2fw1 (wt *Aa*PurE, pH 8.5), 2fw6 (H59N-*Aa*PurE, pH 5.4), 2fw7 (H59N-*Aa*PurE, pH 8), 2fw8 (H89G-*Aa*PurE, pH 8), 2fw9 (H59F-*Aa*PurE, pH 8), 2fwa (H89N-*Aa*PurE, pH 7), 2fwb (H89F-*Aa*PurE, pH 8), 2fwi (H59D-*Aa*PurE·AIR, pH 7), 2fwj (wt *Aa*PurE·AIR, pH 7), and 2fwp (H59N-*Aa*PurE·isoCAIR·citrate, pH 5.4). Figures were prepared using Molscript (*28*), Raster3D (*29*), and PyMOL (*30*).

RESULTS

Identification of A. aceti purE and purK. Attempts to construct and sequence *A. aceti* 1023 genomic libraries yielded a sequence from the *purE* gene (191 bp) that was in turn used to design gene-specific PCR primers and an ODN probe. Sequencing of PCR products obtained with primers targeting conserved regions yielded a 1.2 kb contig containing portions of the adjacent *purE* and *purK* genes (C. P. Mill and J. A. Francois, unpublished observations). Two clones containing the complete *A. aceti purE*−*purK* gene cluster were identified: pJK173 was a member of a pUC118 genomic library able to restore prototrophy to *E. coli purE* auxotrophic strain PC0135, while pJK193 was derived from a λ library probed with a gene-specific ODN. The pJK193 plasmid contained a smaller insert than expected (7 not 15 kb). A nearly complete sequence of the pJK193 insert (6842 bp) was deposited in GenBank with accession number DQ059549. The pJK173 insert corresponds to nucleotides 2921−4994 in this entry.

Pairwise comparisons reveal the *Aa*PurE and *Aa*PurK proteins are ∼10% larger than their *E. coli* counterparts. There is 52% identity in PurEs (95 of 182 residues with no internal gaps; *Ec*PurE has 168 residues) and 29% identity in PurKs (114 of 392 residues with multiple internal gaps; *Ec*PurK has 355 residues). *A. aceti purE* has a GTG start codon, and its TGA stop codon overlaps the ATG start codon of *purK*.

Recombinant AaPurE Purification and Characterization. Functional complementation of a *purE* auxotroph showed that the *A. aceti* enzyme is active in *E. coli*. A pET plasmid containing *A. aceti purE* and *purK* (pJK174) overexpressed both proteins at similar levels in *E. coli* (Supporting Information, Figure S1). Ammonium sulfate (AS) fractionation separates the two proteins, as observed in *Ec*PurE−*Ec*PurK co-overexpression (*4*) but the order of precipitation is reversed: *Aa*PurE precipitates at ≤35% AS, whereas *Ec*PurE precipitates in the 60−85% AS fraction; *Aa*PurK precipitates at a higher ammonium sulfate concentration than *Ec*PurK. At low phosphate concentrations, *Aa*PurE passes through hydroxyapatite while *Ec*PurE adheres. Thus both host enzymes are removed during purification of recombinant *Aa*PurE. Overexpression of *Aa*PurE alone (pJK175) furnished enzyme with identical specific activity to that coexpressed with *Aa*PurK; the *Aa*PurE-only method was used for most wild-type and all mutant preparations.

The N-terminal sequence of purified *Aa*PurE was a 3:1 mixture of sequences MMSETAP and SETAPLP, consistent with partial processing by host Met aminopeptidase. (The gene sequence encodes MSETAPLP but the expression constructs add a second Met residue.) On SDS−PAGE, *Aa*PurE has M_r = 21000, comparable to the expected 18.9 kDa (Figure 1). ESI-MS shows peaks with deconvoluted masses of 18864.5 and 18602.5 (each ±2 Da) in an

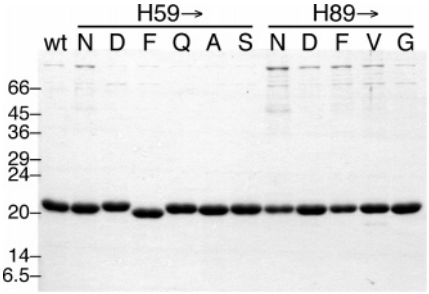

FIGURE 1: SDS−PAGE analysis (15% polyacrylamide, 3 μg each lane) of purified wt and mutant *Aa*PurEs. The positions of molecular mass standards are shown. Each mutation in His59 or His89 is indicated by one-letter code. All proteins had the expected masses by ESI-MS.

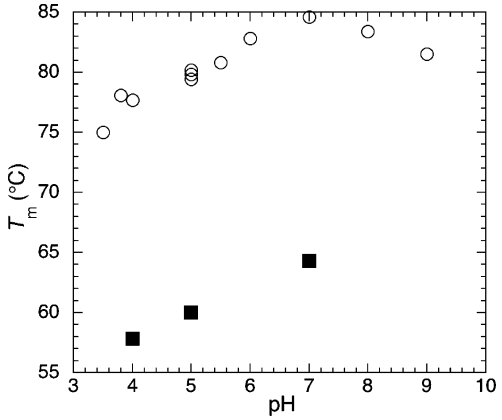

FIGURE 2: *Aa*PurE is thermostable at low pH. Melting temperatures (T_m) were determined by CD thermal unfolding experiments for wt *Aa*PurE (open circles) and *Ec*PurE (filled squares), as a function of pH. Thermal unfolding was monitored using the CD signal at 222 nm and was performed at 0.23 mg/mL for each PurE. At pH 3.5, *Ec*PurE unfolded at the starting temperature (24 °C). Replicate experiments performed at pH 5.0 yielded $T_m = 79.8 \pm 0.4$ °C for *Aa*PurE.

approximately 12:1 ratio, consistent with the full-length protein (Table 1) and the form lacking two N-terminal Met residues (expected difference 262.4 Da), respectively. Gel filtration shows a single peak at 197 kDa, larger than expected for a globular 151.2 kDa octamer. Purified *Aa*PurE has a specific activity of 36 units/mg in the reverse-direction assay that monitors CAIR decarboxylation (pH 8.0, 37 °C, and 0.1 mM CAIR). Under these conditions *Ec*PurE has a specific activity of 40 units/mg with a K_m for CAIR of 36 μM and is an octamer of 17.6 kDa subunits (*4*, *31*). We estimate *Aa*PurK has a specific activity of ~50 units/mg, comparable to the activity of *Ec*PurK (Supporting Information).

Acid Stability Studies. *A. aceti* is an acidophile that tolerates an acidic cytoplasm (*12*). Thus its proteins should be especially suited to functioning at low pH. Monitoring thermal denaturation by circular dichroism is a readily accessible method to assess *Aa*PurE protein stability as a function of pH. In all cases, temperature-induced unfolding was irreversible, so a slow heating rate was maintained (0.41 ± 0.06 °C/min). *Aa*PurE is maximally stable near pH 7 but is remarkably thermostable even at pH 3.5 (Figure 2). Thermal denaturations performed under the same conditions with *Ec*PurE showed much lower (−20 °C) T_ms at pH 4−7, consistent with lower stability at low pH. At pH 3.5, the unfolding of *Ec*PurE occurred during sample preparation at 24 °C.

The ability of *Aa*PurE to withstand prolonged incubation at low pH at 30 °C (the normal organismal growth temperature) provides a second measure of protein acid stability. This experiment has provided evidence for the particular acid stability of *A. aceti* citrate synthase and alanine racemase compared to the equivalent enzymes from nonacidophilic sources (*61*). Small enzyme aliquots were withdrawn from an acidic incubation mixture and assayed for residual enzymatic activity over time. Parallel experiments were performed on *Ec*PurE. We found that *both* forms of PurE began to refold quickly in the pH 8.0 activity assay buffer, which prevented the construction of an inactivation plot.

PurE−Ligand Interaction Studies. Two available PurE structures contain an organic ligand bound to the active site. The first is *Ec*PurE bound to a mononucleotide derived from CAIR (PDB code 1d7a), which shows relatively weaker electron density in the aminoimidazole region than in the ribose 5′-phosphate (R5P) moiety. The PDB entry contains a modeled AIR nucleotide, but the bound species could be AIR (±CO_2), CAIR, N^5-CAIR, or a mixture of these species. Only half of the active sites, on one face of the *Ec*PurE octamer, contained ligands (*2*). Citrate was found in the active site of *Aa*PurE crystallized from 90 mM citrate at pH 5.25−5.5 (*13*). We briefly compare the modes of ligand binding here to introduce key residues. The citrate C1 carboxylate (*pro-R* arm) interacts with *Aa*PurE Ser30 (ordinarily bound to a R5P moiety phosphate O), Asp33

Table 1: Properties of wt and Mutant PurEs

	relative k_{cat}/K_m[a] (units/mg)[b]	k_{cat} (s^{-1})[a]	$K_{m,CAIR}$ (μM)[a]	$K_{d,CAIR}$ (μM)[a]	$K_{d,cit}$ (mM)[c]	MW[d] (calc)
wild type	1[e](39)	12.2 ± 0.6	8.0 ± 1.2		0.4 ± 0.04	18865 (18865.8)
H59N	0 (<0.0005)	nd[f]	nd	0.78 ± 0.07	1.2 ± 0.1	18842 (18842.7)
H59D	0.0016 (0.33)	0.49 ± 0.03	200 ± 30		7.1 ± 1.0	18844 (18843.7)
H59F	0 (<0.0005)	nd	nd	0.46 ± 0.09	0.8 ± 0.3	18875 (18875.8)
H59Q	0.000014 (0.00082)	0.0006 ± 0.0001	30 ± 20		2.8 ± 0.7	18856 (18856.8)
H59A	0 (<0.0001)	nd	nd	0.08 ± 0.02	>10	18799 (18799.7)
H59S	nd (0.0001)[g]	nd	nd		>10	18815 (18815.7)
H89N	0.029 (0.11)	0.063 ± 0.002	1.4 ± 0.2		2.6 ± 0.4	18841 (18842.7)
H89D	0.044 (1.7)	0.40 ± 0.02	6 ± 1		2.7 ± 0.4	18844 (18843.7)
H89F	0.14 (5.8)	1.97 ± 0.09	9 ± 1		2.1 ± 0.2	18875 (18875.8)
H89V	0.17 (5.7)	2.10 ± 0.09	8 ± 1		0.49 ± 0.04	18828 (18827.8)
H89G	0.91 (1.6)	0.97 ± 0.06	0.7 ± 0.5		2.5 ± 0.3	18785 (18785.7)

[a] Determined at pH 8.0 and 30 °C. [b] Determined at 0.1 mM CAIR. [c] Determined at pH 5.3 and 25 °C. [d] Molecular weight observed by ESI-MS (expected MW in parentheses). Experimental uncertainty ±2 Da. [e] wt $k_{cat}/K_m = 1.5 \times 10^6$ M^{-1} s^{-1} at pH 8.0 and 30 °C. [f] nd, not determined. [g] Activity is too low for the reliable determination of kinetic constants.

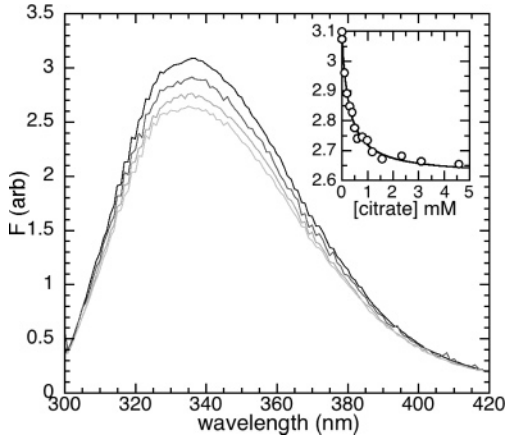

FIGURE 3: Fluorescence titration of wt *Aa*PurE with citrate. Fluorescence emission spectra (excitation 295 nm) for 3 μM wt *Aa*PurE [subunit] in the presence of 0 (black line), 0.2 (67% gray line), 0.6 (36% gray line), and 20 (26% gray line) mM citrate, recorded at 25 °C and a final pH of 4.62, Inset: Diminution of fluorescence emission intensity at 337 nm versus [citrate]. The solid line represents a fit of the data to eq 3, yielding $K_d = 0.28 \pm 0.02$ mM, $\Delta F = 0.468 \pm 0.005$, and $F_o = 3.086 \pm 0.008$.

(ordinarily bound to the R5P 2′- and 3′-hydroxyls), and Gly85 NH (ordinarily bound to the R5P 3′-hydroxyl). The rest of the citrate ion interacts with different parts of the active site than those bound by the mononucleotide: the central carboxylate (C6) interacts with His59 N^{δ} and the C5 carboxylate (*pro-S* arm) interacts with the Gly29 O. Citrate does not contact Ser57, which binds N3 in aminoimidazole rings, or Arg60, which binds the R5P phosphate.

Given the extensive interactions between citrate and the *Aa*PurE active site, citrate titrations were used to determine if the active site structures of mutant *Aa*PurEs were retained at low pH. One advantage of citrate as a nonsubstrate, active site specific probe is its stability at low pH, while CAIR, AIR, and N^5-CAIR have varying degrees of instability. The addition of citrate leads to a progressive decrease in the intrinsic fluorescence emission intensity of *Aa*PurE, presumably due to one or more of the three Trp present (Figure 3). This observation was used to determine the K_d of citrate at various pH values. A rather sharp bell-shaped optimum near pH = 4.6 was observed (Figure 4), consistent with binding of citrate mono- or dianion ($pK_1 = 3.13$; $pK_2 = 4.76$; $pK_3 = 6.80$) (*21*). The log(K_a) vs pH plot has a slope of 0.9 ± 0.1 at pH $\leq$4.6, and a slope of -0.7 ± 0.1 at pH >4.6, indicating that on each arm of the curve a change in the protonation state of a single group is involved in the loss of binding affinity. If one assumes that only dianionic citrate ($pK_2 = 4.76$) binds *Aa*PurE, the curve can be fit to two p*K*s (3.77, 5.18) that probably derive from protein. In this case, the citrate dianion·*Aa*PurE complex would have $K_d = 0.19 \pm 0.01$ mM.

Other common acid metabolites were screened for PurE binding near the optimal pH for citrate binding. None of the other 13 carboxylate compounds tested bound as strongly to *Aa*PurE (Table S2), although isocitrate, fluorocitrate, and malic acid showed measurable K_ds $\leq$4 mM, as determined by fluorescence quenching titrations. The addition of *cis*- and *trans*-aconitate caused an initial increase or decrease, respectively, in *Aa*PurE fluorescence emission intensity. None of these affinities are high enough to suspect that *Aa*PurE is regulated by in vivo carboxylic acid binding.

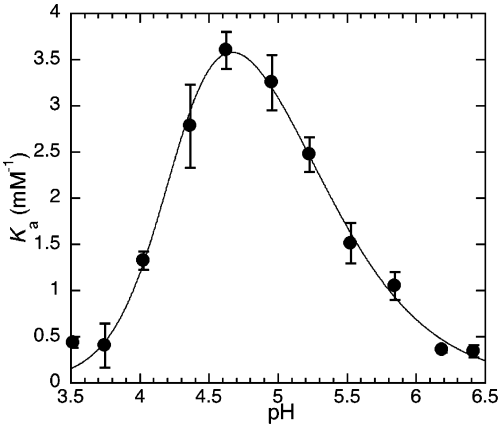

FIGURE 4: pH dependence of wt *Aa*PurE citrate affinity (K_a). Equilibrium constants were determined at 0.3 pH unit increments from pH 3.4 to pH 6.4. Fluorescence titrations were performed at 25 °C using wt *Aa*PurE. The pH was taken as the final value; in no case did this vary from the starting value by more than 0.11 pH unit. The solid line is a fit of the data to eq 5, with $pK_1 = 3.8 \pm 0.1$, $pK_2 = 5.2 \pm 0.1$, and maximum $K_a = 5.3 \pm 0.4$ mM^{-1}.

Mutagenesis of Conserved PurE Residues His59 and His89. The strictly conserved residues His59 (*Ec*PurE His45) and His89 (*Ec*PurE His75) are the only polar residues in or near the active site without a clear role in substrate binding. These residues are found in two highly conserved sequence motifs, named the "forties loop" and the "seventies loop" after the *Ec*PurE residue numbers. The seventies loop shows two differentially conserved sequences that are used to distinguish class I and class II PurEs (using N^5-CAIR or AIR/CO_2 substrates, respectively). His45 N^{δ} is near the aminoimidazole ring in the *Ec*PurE·mononucleotide structure 1d7a, where it could be involved in proton transfers. *Aa*PurE residues His59, His89, His89′, and His59′ (the prime indicates a residue from a second subunit) form a staggered stack of side chains that link two active sites in adjacent monomers, leading to speculation that they might function as a proton channel or signaling apparatus (*13*).

Eleven proteins mutated at His59 or His89 were isolated using the wt *Aa*PurE isolation procedure (Figure 1). His59 is clearly important for activity, since only the H59D-*Aa*PurE and H59Q-*Aa*PurE mutants showed kinetically characterizable activity (Table 1). H59S-*Aa*PurE had activity too low for the reliable determination of kinetic constants, and three mutants (H59N, H59A, and H59F) had no detectable activity at pH 8 and 0.8 mg/mL (40 μM [subunit]). The maximum residual catalytic activities for these inactive mutants (Table 1) were determined from detection thresholds; maximal activities ranged from <0.0003 to <0.0008 unit/mg. (These experiments also confirm that all detectable host *Ec*PurE is removed by the protein purification method.) For H59N-*Aa*PurE, there was no detectable activity in the range pH 5−8 with 0.8 mg/mL enzyme. It appears that there is a real difference between the totally inactive H59N-*Aa*PurE and the barely active H59Q-*Aa*PurE.

All His89 mutants retain some catalytic activity. Several His89 mutants approach wt k_{cat}/K_m, notably H89G-*Aa*PurE, a very nonconservative mutation. At CAIR concentrations above $2K_m$, mild apparent substrate inhibition was observed with H89F-*Aa*PurE. Since H89F-*Aa*PurE is somewhat "overpacked" in the region between adjacent active sites, this may indicate some negative cooperativity in substrate binding,

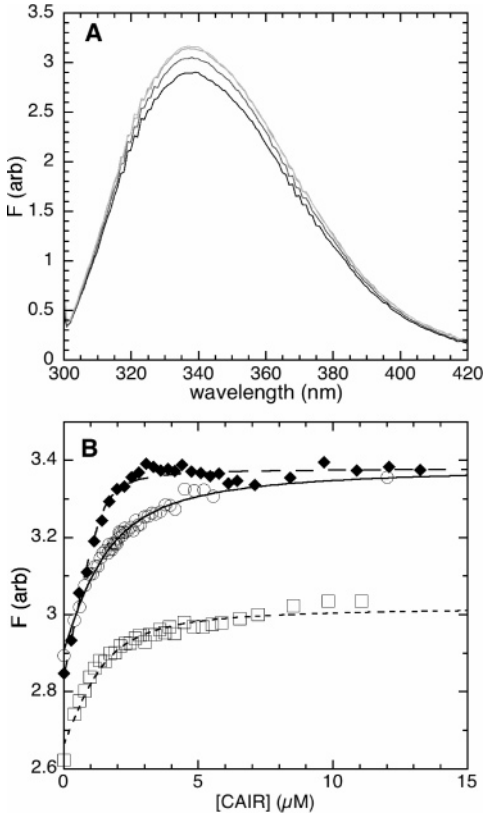

FIGURE 5: Fluorescence titration of inactive *Aa*PurE mutants with CAIR. (A) Fluorescence emission spectra obtained at 0 (black line), 0.78 (67% gray line), 2.2 (36% gray line), and 19 (26% gray line) μM CAIR with 2.7 μM H59N-*Aa*PurE [subunit], recorded at 25 °C with excitation at 295 nm. The final pH for this experiment was 7.99. (B) Fluorescence emission intensity at 338 nm versus [CAIR] for H59N-*Aa*PurE (open circles), H59F-*Aa*PurE (open squares), and H59A-*Aa*PurE (filled diamonds). Titrations were performed at 2.7, 2.9, and 2.9 μM *Aa*PurE [subunit], respectively. Lines are fits to eq 4 with $K_{d,CAIR} = 0.78 \pm 0.07$ μM, $\Delta F = 0.479 \pm 0.009$, and $F_o = 2.909 \pm 0.007$ for H59N-*Aa*PurE; $K_{d,CAIR} = 0.46 \pm 0.09$ μM, $\Delta F = 0.36 \pm 0.01$, and $F_o = 2.84 \pm 0.01$ for H59F-*Aa*PurE; and $K_{d,CAIR} = 0.08 \pm 0.02$ μM, $\Delta F = 0.54 \pm 0.01$, and $F_o = 2.84 \pm 0.01$ for H59A-*Aa*PurE.

either when both active sites are occupied or (if the sites are alternately occupied) during the conversion of occupied to vacant sites. Similarly, the nearly complete compensation of a lower k_{cat} by a lower K_m in H89G-*Aa*PurE suggests that wt *Aa*PurE might use steric strain to cause ground-state destabilization and increase k_{cat}.

Since both His59 and His89 are in or near the active site, K_ds were determined for citrate (at pH ≈5, all mutants) and CAIR (at pH 8, fully inactive mutants) to assess their contributions to ligand binding. The addition of citrate diminishes the intrinsic fluorescence emission from *Aa*PurE (Figure 3), while the addition of CAIR has an opposite effect of an approximately equal magnitude (Figure 5). Titrations with CAIR were performed at 25 °C under conditions that minimized its nonenzymatic decomposition to <7% over the course of the titrations (see below). The CAIR K_ds for inactive mutants were all at least an order of magnitude lower than CAIR K_ms, indicating the substrate could bind to all variant enzymes. Most His59 mutants and all His89 mutants had citrate K_ds equal to or slightly higher than wt *Aa*PurE (Table 1), indicating that the active site remains largely intact. There was no obvious correlation between citrate K_ds and CAIR K_ms (or K_ds for inactive mutants).

Characterization of Strain PC0135. *E. coli* strain PC0135 is a *purE*-deficient strain with a previously unreported molecular lesion (*17*). PCR was used to amplify the entire *purE*−*purK* region from *E. coli* strain PC0135. DNA sequencing showed only one difference from the wt sequence, a point mutation that alters *purE* Trp151 codon TGG to stop codon TGA, which would delete the final helix in *E. coli* PurE and likely prevent octamer assembly. The *purK* gene is intact.

Mutant Functional Complementation Studies. *Aa*PurE His59 mutants were tested for their ability to restore prototrophy to PC0135 and confirm the observed in vitro activities. Because the *purE* mutant strain PC0135 lacks T7 RNA polymerase, mutant plasmids for complementation tests were derived from the pUC118 derivatives pJK173 and pJK324. The former contains full-length *purE*−*purK* and surrounding sequence while the latter contains just *purE* in the same orientation and with the same flanking sequences present in pJK173. *Aa*PurE and *Aa*PurK purified from *E. coli* overexpressers have essentially the same specific activity as their *E. coli* counterparts, leading to the expectation they should functionally complement *E. coli* auxotrophs. As expected, wt and H59D *purE* genes were able to complement the PC0135 auxotrophy on solid or liquid medium, but surprisingly *A. aceti purK* was also required (Table 3). Unexpectedly, the H59N-*Aa*PurE mutant strain also grew, albeit very slowly, in conditions that did not allow growth of a pUC118 control. Thus H59N-*Aa*PurE may have a very low (spectroscopically undetectable) activity, or its reaction in vivo is somehow affected by high pCO_2. Cells expressing only wt *Aa*PurE (pJK324) required the high CO_2 conditions of a candle jar. At high CO_2, TX209 (*E. coli purK*223, a Tyr147 → Ter mutant) (*4*) can bypass its mutation. Hence PurK or high CO_2 can provide carboxylated AIR for further biosynthesis. These results indicate that *Aa*PurE and *Aa*PurK are able to function together in *E. coli* but suggest that *Aa*PurE is unable to accept N^5-CAIR produced by *E. coli* PurK.

Structures of PurE Forms at Low and High pH. All tested forms of *Aa*PurE crystallized readily in the same crystal form observed previously (*13*). Ten different wt and mutant *Aa*PurE structures were determined; data collection and refinement statistics are presented in Tables 2 and S3 (Supporting Information). The original (1u11) *Aa*PurE·citrate complex structure was solved at low pH. A structure of wt *Aa*PurE solved in the absence of citrate at pH 8.5 (2fw1) showed no substantive differences near the active site. However, a planar anion modeled as acetate was bound by the side chain of Asp33 and the backbone NH of Gly85, in the same approximate location as the nucleotide substrate 3′-hydroxyl. In sum, the structure of *Aa*PurE is largely unaffected by both pH and citrate binding.

Is There a Proton Channel Linking Active Sites? PurE is an octamer in the crystal and in solution. Active sites in subunits A and D are related by a molecular 2-fold axis and are linked by a series of four absolutely conserved His residues, His59, His89, and their symmetry-related partners His59′ and His89′. This His chain looks like it could function to shuttle protons between two active sites as a relay on the imidazole nitrogens (*13*), analogous to a Grotthus proton conduction mechanism (*32*). Since His59 is largely isolated from solvent by the bound substrate, a proton channel might allow for its protonation or deprotonation in an occupied

Table 2: Crystallographic Data and Refinement Statistics

	wt (pH 8.5)	wt·AIR (pH 7)	H59D·AIR (pH 7)	H59N·cit (pH 5.4)	H59N·isoCAIR·cit (pH 5.4)
PDB code	2fw1	2fwj	2fwi	2fw6	2fwp
cell dimensions (space group *I*422)	$a = b = 99.4$ Å; $c = 164.2$ Å; $\alpha = \beta = \gamma = 90°$	$a = b = 99.2$ Å; $c = 164.4$ Å; $\alpha = \beta = \gamma = 90°$	$a = b = 99.0$ Å; $c = 163.8$ Å; $\alpha = \beta = \gamma = 90°$	$a = b = 98.6$ Å; $c = 165.5$ Å; $\alpha = \beta = \gamma = 90°$	$a = b = 98.7$ Å; $c = 165.5$ Å; $\alpha = \beta = \gamma = 90°$
resolution (Å)	50−2 (2.07−2.00)[a]	40−1.95 (2.02−1.95)	40−1.95 (2.02−1.95)	50−1.85 (1.92−1.85)	50−1.85 (1.92−1.85)
reflections (total/unique)	155660/28092	167074/30068	160170/30234	298445/33762	194365/33580
completeness (%)	99.4 (98.6)[a]	99.2 (97.1)	99.8 (100.0)	95.9 (80.3)	95.2 (77.4)
$\langle I/\sigma \rangle$	27.0 (4.8)	23.4 (3.6)	22.7 (3.8)	36.0 (3.5)	24.7 (2.3)
R_{sym}[b] (%)	5.6 (33.5)	6.4 (49.4)	6.6 (51.8)	5.5 (38.9)	5.0 (29.8)
R_{cryst}[c]/R_{free}[d] (%)	16.7/18.5	19.1/20.2	16.4/19.1	17.2/18.7	19.7/22.2
no. of protein atoms	2318	2309	2323	2333	2314
no. of water molecules	311	198	285	335	316
no. of ligand ions	2	1	1	1	2
rmsd, bond lengths (Å)	0.005	0.007	0.013	0.005	0.005
rmsd, bond angles (deg)	1.3	1.3	1.3	1.3	1.3
average *B*-factor (Å^2)	24.0	21.4	23.4	23.6	25.2

[a] Numbers in parentheses refer to highest resolution shell. [b] $R_{sym} = \sum|I_h - \langle I_h \rangle|/\sum I_h$, where $<I_h>$ is the average intensity over symmetry. [c] $R_{cryst} = \sum|F_o - \langle F_c \rangle|/\sum F_o$, where the summation is over the data used for refinement. [d] R_{free} is defined the same as R_{cryst} but was calculated using 5% of the data excluded from refinement.

Table 3: Functional Complementation Studies in *E. coli* PC0135 (*purE*)

plasmid (*A. aceti* genes)	MM (solid) + hypoxanthine[a]	MM (solid)	MM (solid) + high CO_2[b]	MM (liq)
pJK173 (PurE/PurK)	+++[c]	+++	++	+++
pJK347 (H59D-PurE/PurK)	++	++[d]	nd	+[d]
pJK348 (H59N-PurE/PurK)	++	+[d]	+	−
pJK324 (PurE)	++	−	+	−
pJK346 (H59D-PurE)	++	−	−	−
pJK340 (H59N−PurE)	++	−	−	−

[a] Minimal medium (MM) defined in Experimental Procedures. Hypoxanthine was added at 15 μg/mL (0.1 mM). [b] Plates were placed in a candle jar (see Experimental Procedures). [c] Key to symbols: +++, large colonies/saturated culture at 24 h; ++, small colonies at 24 h; +, small colonies/light turbidity at 72 h; −, no growth observed at 144 h; nd, not determined. [d] The indicated plasmid was recovered from this culture, and its DNA sequence was obtained to confirm that the *purE* region had not been modified.

active site. This would add to the number of mechanisms that must be considered for an isolated active site. One possibility is that only half of the PurE active sites might function at any one time. Some circumstantial support for this idea comes from nucleotide·PurE crystal structures: there is no evidence for simultaneous occupancy by a nucleotide of more than four active sites, and these are always on the same "face" of the octamer. Finally, there is no His89 equivalent in class II PurEs, which use different substrates than class I PurEs and release a proton together with the CAIR product, so should have at least subtle differences in proton transfers.

The replacement of buried, conserved residues His89/His89′ with neutral residues did not eliminate *Aa*PurE activity (Table 1), indicating that ionizable residues are unnecessary. However, two pairs of waters were observed on either side of His89/His89′, which might still allow the active sites to be linked by a Grotthus proton chain. Structures were solved for H89G-*Aa*PurE (2fw8), H89N-*Aa*PurE (2fwa), and H89F-*Aa*PurE (2fwb) mutants in the absence of ligands. These variants represent a range of protein underpacking to overpacking at position 89 and demonstrate that the PurE structure is rigid and robust in this region between active sites. Remarkably few alterations in protein structure were noted (Figure S4 in Supporting Information). In H89G-*Aa*PurE only a slight backbone rotation in Ala88 was observed, with waters occupying the new cavity. H89F-*Aa*PurE has the Phe rings stacked on each other, which seals any direct route between active sites in subunits A and D. However, all solved structures still contain the two water pairs on either side of the symmetry-related residue at position 89. These isolated waters are deeply buried in the protein, make polar contacts only to backbone atoms, and are far from any ionizable group. We conclude that even if the His59/His89 residues formed a proton channel linking *Aa*PurE active sites, it has no required role.

Extinction Coefficients for Enzyme Assays. As a first step in the construction of a pH−rate profile, we used end point assays to determine $\Delta\epsilon_{260}$ values for the conversion of CAIR → N^5-CAIR at various pH values. This method accounts for changes in absorbance due to N^5-CAIR decarboxylation to AIR on the time scale used for enzyme activity determinations and avoids the need to obtain "clean" spectra of acid-labile carboxylated nucleotides at many acidic pHs. The data shown in Figure S2 (Supporting Information) were used to interpolate extinction coefficients in the pH range 5.0−8.0: $\Delta\epsilon_{260} = 1.19(\text{pH} - 0.15)$. Outside this range, individual $\Delta\epsilon_{260}$ values were determined for each pH used.

pH−Rate Profiles. The k_{cat}/K_m versus pH profiles (Figure 6A) are similar bell-shaped curves for both wt and H59D-*Aa*PurE ($pK_1 = 6.0 \pm 0.1$ and 5.7 ± 0.2, respectively; $pK_2 = 7.2 \pm 0.1$ and 6.5 ± 0.2, respectively). Fitting of the wt profile required eq 2, which assumes that two ionizations occur at pK_1. The origin of this second pK_1 in wt but not H59D-*Aa*PurE is considered in the Discussion.

The k_{cat} versus pH profiles (Figure 6B) are also bell-shaped but differ in appearance for wt and H59D-*Aa*PurE ($pK_1 = 5.1 \pm 0.2$ and 4.4 ± 0.4, respectively; $pK_2 = 8.4 \pm 0.1$ and 6.8 ± 0.2, respectively).

The different pK_2 values obtained for wt and H59D-*Aa*PurE in each pH−rate profile correspond to the differing acidities of the His and Asp side chains, indicating that the basic arm in the enzyme−substrate complex is determined by the protonation state of residue 59. At higher pH, the Asp59 mutant may electrostatically repel the carboxylates in CAIR and N^5-CAIR.

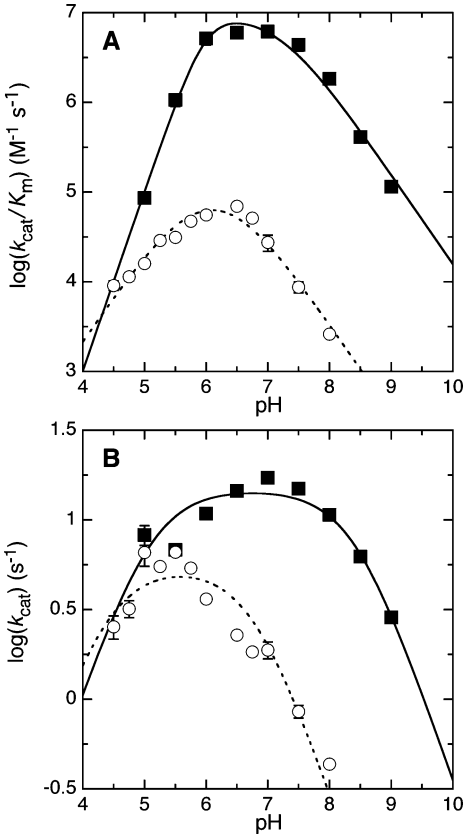

FIGURE 6: pH−rate profiles for wt *Aa*PurE (solid squares) and H59D-*Aa*PurE (open circles). (A) k_{cat}/K_m versus pH. (B) k_{cat} versus pH. Values and errors were determined from initial velocity data obtained at 30 °C and the indicated pHs, fit to the Michaelis−Menten equation. The lines are fits of each pH−rate data set to eq 1, except in panel A, where the wt data are fit to eq 2. Ionization of wt His89 is proposed to be the cause of the "second pK_1" in the wt k_{cat}/K_m profile (see Discussion).

The acidic arms for the wt and H59D-*Aa*PurE profiles are similar, indicating that His59 does not affect pK_1. In addition, the similar pK_1 values in the k_{cat} and k_{cat}/K_m plots would suggest that pK_1 corresponds to an enzyme moiety involved in substrate binding. However, this assumes the substrate does not ionize to a form that cannot bind productively. In this case, the pK_a for CAIR N3 is 6.11 at 30 °C (*33*); CAIR·H^+ might not bind *Aa*PurE well, as all PurE·nucleotide crystal structures indicate that a hydrogen bond forms between Ser57 and N3. This interaction would also make CAIR N3 more difficult to protonate in the enzyme−substrate complex, explaining the lower pK_1 in the k_{cat} profile. Protonation of the substrate phosphate moiety (pK_2 for R5P = 6.3 (*34*)) is also a possibility. If an enzyme moiety is involved, the best candidate for pK_1 is Asp33, which is critical for ribose binding.

The apparently nonconservative Asp mutant is a surprisingly efficient enzyme, with maximal k_{cat} equal to ~40% of wt maximal k_{cat}. Since pK_1 and pK_2 are closer together for H59D-*Aa*PurE, the actual maximal mutant k_{cat} is likely closer to 55% of wt. At pH 8, the $K_{m,CAIR}$ for H59D-*Aa*PurE is 25-fold higher than wt *Aa*PurE and k_{cat}/K_m for H59D-*Aa*PurE is 10^2-fold smaller, consistent with an expectation that this mutant would electrostatically repel the anionic substrate. Citrate shows a similarly lower affinity, a 18-fold increase in K_d for wt → H59D.

Nucleotide−AaPurE Complex Structures. Crystal soaking at a range of pH values yielded several structures of CAIR-derived nucleotides bound to *Aa*PurE. Soaks with active *Aa*PurE would be expected to contain a mixture of nucleotide species affected by the pH and CO_2/bicarbonate levels. At the lower pH values used, some nonenzymatic decarboxylation of CAIR is expected. Three liganded crystal structures were refined to R_{free} = 22% using diffraction data extending to at least 2.0 Å resolution. The asymmetric unit contains a dimer. Four dimers related by the crystallographic 4-fold axis form the biologically relevant *Aa*PurE octamer, which pack into tightly associated pairs in the crystal lattice. Partial occupancy of only the outward-facing active sites was observed for all liganded structures, suggesting that diffusion within the crystals is limited by this packing arrangement.

wt AaPurE·AIR (2fwj). This pH 7 structure shows nucleotide on one face of the octamer. Continuous electron density defines the nucleotide as AIR (Figure 7A). The mode of binding is similar to that observed in the *Ec*PurE·nucleotide structure (1d7a), with the Ser57 hydroxyl contacting AIR N3, Ser30 and Arg60 contacting the phosphate oxygens, and Asp33 binding both ribose hydroxyls. *Ec*PurE showed higher temperature factors in the aminoimidazole region relative to the R5P moiety. In the 2fwj structure, temperature factors for the aminoimidazole ring average 42 Å^2, comparable to the 39 Å^2 average for the R5P moiety (surrounding side chains average 19 Å^2, backbone atoms 19 Å^2). His59 Nδ is 3.4 Å from and directly above AIR C4, with the aminoimidazole ring wedged slightly under the His59 ring. The protein conformation is essentially the same as wt *Aa*PurE at pH 8.5 (2fw1) or pH 5.5 (1u11), apart from an inward rotation of Arg60 to bind the AIR phosphate.

H59D-AaPurE·AIR (2fwi). The structure of the low pH active mutant H59D-*Aa*PurE was determined at pH 7 with clear density for AIR in active sites on one face of the octamer. This pH is near the optimum for wt *Aa*PurE but is well down the basic arm of the k_{cat} vs pH profile for H59D-PurE. Again, the pH of the soaking solution allows sufficient decarboxylation, possibly via N^5-CAIR, to form AIR. The Asp59/Arg60 region adopts at least two conformations, one in which the Asp59 side chain interacts with His89 and one with the Asp59 side chain pointed at the C4 of the bound AIR. The orientations are related by an ~60° rotation around the Cα−Cβ bond, with little rotation of the carboxylate. Only the first orientation is clearly compatible with the presence of AIR: one Asp59 side chain O atom is 3.0 Å from His89 Nδ and the other is 3.0 Å from AIR C4. Again, Ser57 interacts with AIR N3, which appears to limit base rotation around the glycosidic bond. As a consequence, the exocyclic N atom is likely too far from Asp59 (3.7 Å) to form a hydrogen bond. The only major structural difference between wt·AIR (2fwj) and H59D·AIR (2fwi) is the inwardly rotated Asp conformer in the first orientation.

H59N-AaPurE·isoCAIR (2fwp). Structures solved for apo H59N-*Aa*PurE at pH 5.4 (2fw6) and 8 (2fw7) show few pH-dependent changes. A complexed structure was obtained by soaking a low pH grown H59N-*Aa*PurE crystal with CAIR prior to data collection. After refinement of the unliganded structure against the diffraction data for the complex, $2F_o - F_c$ electron density maps revealed clear, continuous density for a nucleotide in the active site (Figure 7B). This nucleotide was initially modeled as AIR; however, additional unam-

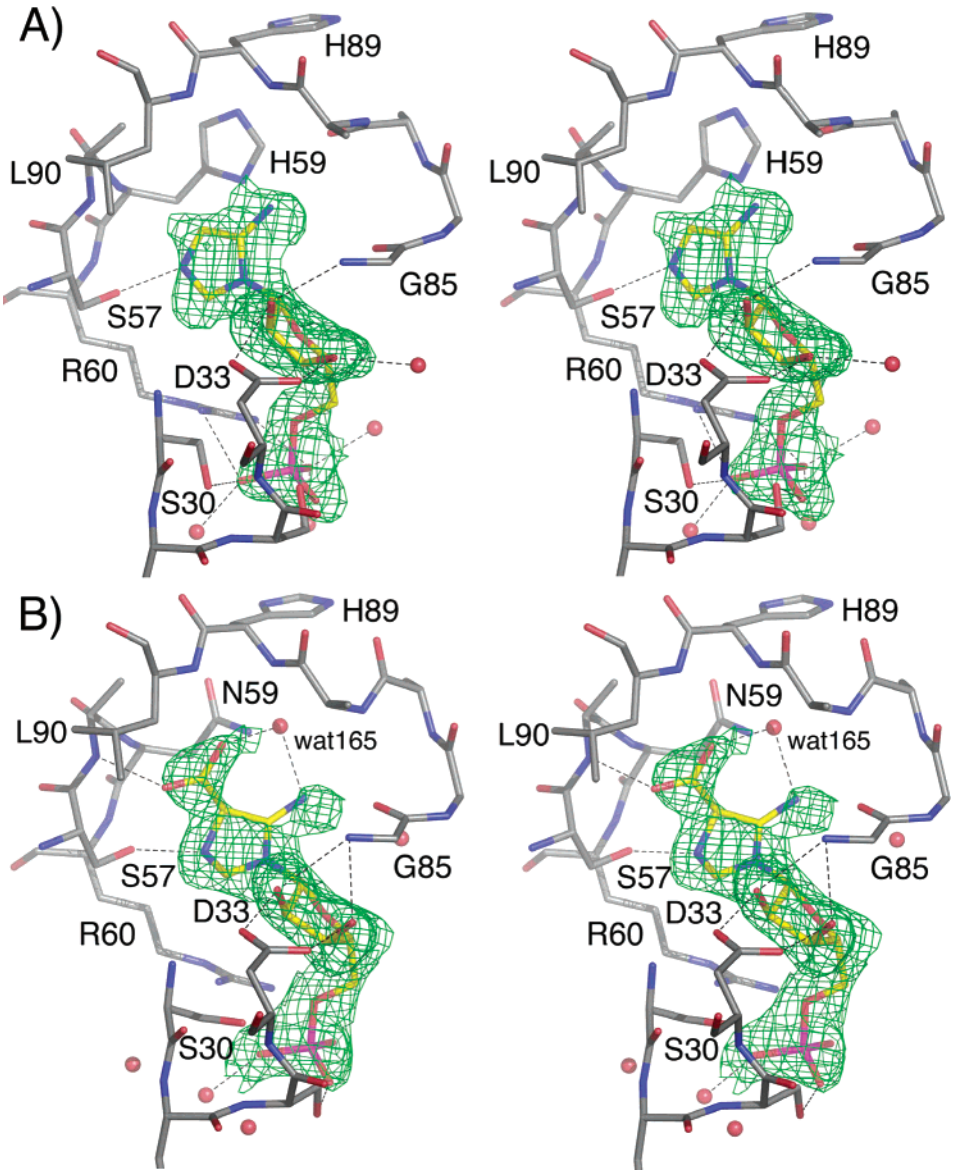

FIGURE 7: Crystallographic characterization of ligand-bound *Aa*PurE structures. Divergent stereo diagram of the σA-weighted $2F_o - F_c$ omit maps (*60*) for the wt *Aa*PurE·AIR complex (A, PDB code 2fwj) and the H59N-*Aa*PurE·isoCAIR complex (B, PDB code 2fwp). Omit maps were calculated using the final refined structure with the nucleotide omitted and are contoured at 1σ (A) or 0.7σ (B). For clarity, electron density is illustrated only for the nucleotide.

biguous electron density not accounted for by the AIR model was observed extending from C4. This additional electron density had a shape consistent with a carboxylate group but was located above the plane of the ring, which is inconsistent with the carboxylate group in CAIR or N^5-CAIR. Rather, the angle at which the extra electron density extended from the ring indicated sp^3 hybridization at C4. The nucleotide was therefore modeled as an isomer of CAIR, 4(*R*)-carboxy-5-iminoimidazoline ribonucleotide (isoCAIR). In this structure, the C4 position of CAIR has been protonated on the *re* face, which causes the carboxylate moiety to move into a largely hydrophobic pocket defined by the "seventies loop". However, the carboxylate contacts backbone NHs in Val56, His89, and Leu90 (2.7, 3.0, and 3.1 Å, respectively). One carboxylate oxygen and the exocyclic nitrogen are in hydrogen-bonding range to water 165 (2.6 and 2.5 Å, respectively). Other contacts to the nucleotide, most notably Ser57 Oγ−N3 (2.6 Å), are the same as in the AIR complexes. A notable difference is the position of the backbone carbonyl in Ala87, which points away from isoCAIR [$\psi_{87} = -19°$ and $\phi_{88} = +34°$; the wt·AIR structure (2fwj) shows $\psi_{87} = +78°$, $\phi_{88} = -77°$, and a 3.1 Å contact between Ala87 O and the AIR exocyclic N]. The heterocycle is no longer planar, with a slight motion of N3 out of the plane defined by the other atoms and an sp^3 hybridized C4 (109.7° angle defined by C5−C4−carboxylate). The modeled position of the exocyclic nitrogen N6 is slightly shifted from the tube of electron density, which is ~0.5 Å closer to the N1 position. The fit of N6 could be improved by increasing the C4−C5 bond length or decreasing the N1−C1′ bond length; neither of these changes would be consistent with chemically plausible structures, however. Further, multiple conformations are unlikely, as the ribose ring and phosphate group are clearly positioned in the electron density; any additional conformations would therefore have to arise from rotation about the C1′−N1 bond. This rotation would not improve the fit of N6 and would disrupt the fit of the carboxylate group to its electron density. The model of

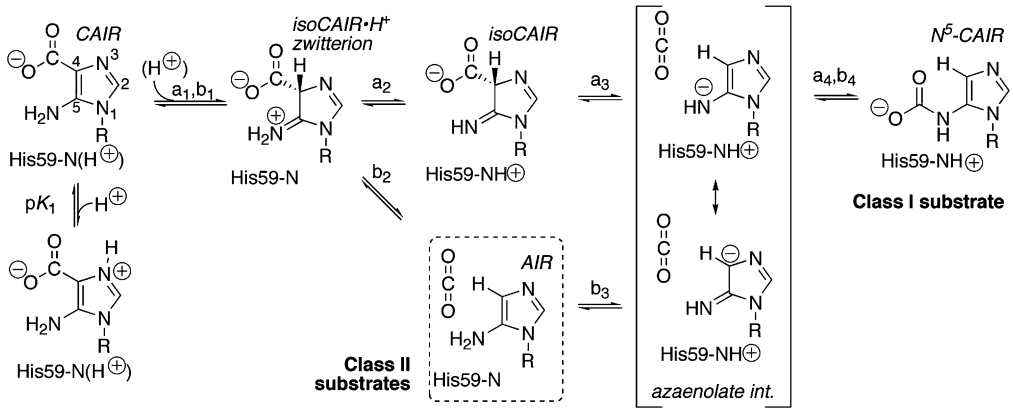

FIGURE 8: Mechanistic possibilities for the class I PurE reverse direction (CAIR → N^5-CAIR). Protonation at CAIR N3 forms an unproductive zwitterion (pK_1 in the k_{cat} vs pH profile). For one or more of the steps a protonated His59 is essential (pK_2). Initial protonation at C4 by an unidentified general acid is followed by deprotonation of the exocyclic imino group (mechanism a, step 2, a_2) or C−C bond cleavage (b_2). The next step forms a resonance-stabilized azaenolate anion (a_3, b_3) that can either form N^5-CAIR (a_4, b_4) or revert to an earlier intermediate. Reverse reactions are denoted in the text with negative subscripts, e.g., step b_{-3}. Concerted reactions are possible (e.g., a_1/a_2). The putative class II PurE substrates are formed during mechanism b (dashed box). The H59N-*Aa*PurE•isoCAIR(•H^+) complex is blocked at step a_2, b_2, or a_3.

isoCAIR presented here, therefore, respresents the most plausible chemical structure that best accounts for the available data. Eliminating most exotic alternatives (e.g., substitution of the 5-imino position by a nucleophile, hydrogen-bonding to the anomeric proton, etc.), it is also not clear if this low pH structure represents a neutral imino moiety (isoCAIR), protonated iminium moiety (isoCAIR•H^+ zwitterion), or a mixture of the two. We have modeled it as a neutral imino species because of two assumptions: deprotonation of the CAIR exocyclic amine would facilitate protonation at C4, and the isoCAIR•H^+ zwitterion would have a lower barrier to decarboxylation.

DISCUSSION

We hypothesize that cytoplasmic enzymes from *A. aceti* have been subject to strong evolutionary selection for acid resistance in the low-pH conditions routinely encountered within the organism. Our goal is to determine if pure *A. aceti* enzymes are intrinsically resistant to acid-mediated inactivation, and if so, how they are structurally and functionally adapted. An analogous situation is the observed thermoadaptation of thermophile proteins. It is also interesting to consider what happens to metabolic networks and metabolite pools in acidophiles during periods of cytoplasmic acidification, which might hamper biosynthesis or speed decomposition of needed compounds. Metabolite channeling or other strategies to protect labile intermediates could be employed as an environmental adaptation (*1*). The genetic evidence presented here hints at a requirement for *Aa*PurK in the proper functioning of *Aa*PurE in a *purE*-deficient *E. coli* strain, and experiments to confirm the implied protein−protein interaction are planned.

We previously compared PurE structures from a mesophilic acidophile (*A. aceti*), mesophilic neutralophile (*E. coli*), and thermophilic (~80 °C) neutralophile (*T. maritima*) (*13*).[2] While one might anticipate *Aa*PurE to be more like *Ec*PurE, a 52% identical protein from another Gram-negative bacterium, the *Aa*PurE surface charge decorations, hydrogen-bonding interactions, and other features were more reminiscent of *T. maritima* PurE. Specifically, the surfaces of both *Aa*PurE and *Tm*PurE are decorated with a distribution of positively and negatively charged residues. The ability of charged surface residues to stabilize protein structures has received much recent attention (*36*−*40*). Interactions between oppositely charged residues on a protein's surface contribute to its stability, and replacing residues that have unfavorable charge−charge interactions can further stabilize a protein. Also, *Aa*PurE displays more intrasubunit hydrogen bonds than *Ec*PurE (*13*), and its salt bridges involve residues that have hydrogen bonds that are shorter and have more nearly ideal geometry than those from *Ec*PurE. All *Aa*PurE salt bridges are at the protein's surface, minimizing the desolvation energy expended to form the interaction. While salt bridges are generally destabilizing, they are most likely to contribute to stability when they are near the protein surface and when the residues involved are part of a network of energetically favorable polar interactions (*41*, *42*). The high T_ms observed here are consistent with the generally "thermophilic" appearance of *Aa*PurE. (While the thermal stability of *T. maritima* PurE is unknown, it is reasonable to expect it to be at least as stable as *Aa*PurE.) *Ec*PurE is much more susceptible to thermal unfolding at neutral and low pH, confirming that *Aa*PurE has increased stability. *A. aceti* citrate synthase and alanine racemase are also both thermostable and acid-resistant (*61*). We propose that the uniformly observved thermostability of *A. aceti* proteins, which seems unnecessary for life at 30 °C, is a byproduct of protein acid adaptations.

Previous mechanistic work has demonstrated intramolecular carboxylate migration in the conversion of N^5-CAIR to CAIR, suggesting transient formation of trapped CO_2 and AIR (or a related species) in the active site (*5*). In this study two His residues were mutated in hopes of characterizing proton transfers occurring at the active site. Our results suggested an updated working hypothesis for the reverse-direction (CAIR → N^5-CAIR) PurE mechanism (Figure 8). One striking observation in the crystal structures reported here is how little *Aa*PurE moves, despite stabilizing diverse nucleotide species in a complex, multistep reaction involving labile intermediates.

[2] A second PurE structure from a mesophilic neutralophile, *Bacillus anthracis*, has recently appeared: PDB code 1xmp (*35*).

His89. His89 is part of the seventies loop, a region of differentially conserved sequence in class I and class II PurEs named after the *Ec*PurE numbering. It is part of a four-His chain suggested to be a proton channel or "wire" that might move protons into or out of an occupied active site (*13*), similar in function to carbonic anhydrase His64 (*43*, *44*) or a tunnel in the E1 component of the pyruvate dehydrogenase complex (*45*). However, mutagenesis studies show that *Aa*PurE His89 is clearly nonessential and can be substituted with residues that cannot participate in a proton tunnel between active sites. However, structures of the mutants provide few clues as to why some mutants are not very active. The most active substitution, with nearly wt k_{cat}/K_m, is H89G-*Aa*PurE, in which the imidazole rings are replaced with a handful of waters and the backbone near Ala88 is altered. In this mutant, K_m is ~10-fold lower than wt and similar to $K_{d,CAIR}$ values measured for inactive mutant, suggesting that wt *Aa*PurE exerts some ground-state destabilization on bound nucleotide. The H59N-*Aa*PurE·isoCAIR structure indicates a strong distortion of bound CAIR. In the PurE mechanism proposed by Stubbe (*2*, *5*), ground-state destabilization occurs in the forward direction when nucleotide binding forces the N^5-CAIR carbamate into a hydrophobic pocket, favoring decarboxylation of the carbamate. The H59N-*Aa*PurE·isoCAIR crystal structure (2fwp) indicates that the nucleotide carboxylate (and, transiently, CO_2) will occupy this pocket, which is largely defined by the remainder of the nucleotide, the backbones of the forties and seventies loops, and the side chains of Ala58, Ala88, and Leu90. Most interactions between PurE and AIR (and possibly CAIR or N^5-CAIR) involve the R5P moiety. The binding enthalpy provided by these interactions is clearly important in catalysis; nucleosides are ineffectual substrates or inhibitors for purine biosynthesis enzymes.

His59. His59 is an absolutely conserved forties loop residue that is needed for *Aa*PurE function. An acid or base role is suggested by the observation that one ionizable mutant (H59D) works well but all neutral mutants are inactive or nearly so. Consistently low $K_{d,CAIR}$ values for inactive His59 mutants and the slight steric clash between AIR and His59 in the pH 7 wt *Aa*PurE·AIR structure (2fwj) indicate that His59 does not contribute to high-affinity ligand binding. This contrasts with citrate affinities, which depend in part on a citrate−His59 N^δ interaction. We initially suspected that His59 would have a role in the protonation of CAIR C4 (Figure 8, step 1 in mechanisms a and b). The observation of a protonated C4 in the H59N-*Aa*PurE·isoCAIR structure (2fwp) indicates that H59 is not absolutely required for this function, although it would be ideally positioned to perform it in wt *Aa*PurE. As a consequence, while both the acid responsible for protonating C4 and the initial protonation state of His59 in the CAIR complex are unknown (parentheses in Figure 8), starting with a protonated His59 is attractive because the same enzyme form could be used to bind either CAIR or N^5-CAIR.

Assignment of pKs in the k_{cat} versus pH Profile. *Aa*PurE appears to stabilize the reaction intermediate isoCAIR, formed here by protonation of a carbon α to a carboxylic acid at moderately acidic pH. (This contrasts with the enolase superfamily, a set of enzymes that perform metal-assisted deprotonations (*46*, *47*).) Protonation of CAIR C4 is required for decarboxylation and might seem to be a natural candidate for pK_2 in the k_{cat} pH−rate profile, which reports on ionizations occurring within the enzyme−substrate complex (*48*). However, the shift of this arm of the profile in the His → Asp mutant tends to associate pK_2 more with the residue 59 side chain than the CAIR C4. As discussed above, His59 is not essential for CAIR C4 protonation, which occurs in the H59N-*Aa*PurE crystal (2fwp structure). The crystal pH is similar to the pH range in which H59D-*Aa*PurE is most active, so it is possible that neither Asn59 nor Asp59 has any direct role in protonating CAIR C4. Clearly, pK_2 has some other origin.

Another candidate for pK_2 is the protonated His59 required in the first step of the forward reaction (N^5-CAIR → CAIR), in which C−N bond scission is facilitated by proton transfer (forming AIR·CO_2, steps b_{-4} and b_{-3}) or electrostatic interactions (forming the azaenolate·CO_2 intermediate, step a_{-4}/b_{-4}). The product formed from this intermediate depends on whether CO_2 is attacked by C4 (leading to CAIR) or the exocyclic nitrogen (re-forming N^5-CAIR), which seems equally feasible. Our working hypothesis is that pK_2 corresponds to protonated His59, which is required for formation of the resonance-stabilized azaenolate·CO_2 intermediate, by step a_3 or b_3 (in the latter, His59 functions as a base, not an acid). Protonated Asp is an acceptable substitute but not Asn or Gln, which may mean that the proton is strongly associated with the azaenolate anion or that the azaenolate·CO_2·His59-H^+ exchanges rapidly with AIR·CO_2·His59 (steps b_3/b_{-3}). The wt *Aa*PurE·AIR structure (2fwj) suggests the protonated His59 N^δ would be about equidistant from the exocyclic N or C4 in the azaenolate intermediate.

One apparent problem with this hypothesis is the difference in charge between a protonated His and a protonated Asp. However, Asp59 structures show a hydrogen-bonding interaction to His89 that is not observed in wt *Aa*PurE. Thus, at the low-pH optimum of H59D-*Aa*PurE, neutral Asp59 may interact strongly with both a positively charged His89 and the azaenolate anion, mimicking the His59-H^+−azaenolate interaction in wt *Aa*PurE. The Asp59−His89 interaction would also hamper His89 protonation in H59D-*Aa*PurE. Lacking this interaction, His89 would be more easily protonated in wt *Aa*PurE. We believe this is the likely origin of the "second pK_1" observed in the wt k_{cat}/K_m versus pH profile.

Studies of the nonenzymatic decarboxylation of CAIR and analogues show a transition (pK = 6.11 at 30 °C) between slow reaction at neutral/basic pH and fast reaction at acidic pH (*33*, *49*). This transition was assigned to protonation of CAIR N3 (*50*). Once protonated on N3 (or the exocyclic N), CAIR would be unable to acquire a C4 proton. The current study shows that *Aa*PurE instead directs protonation to CAIR C4, to form isoCAIR(·H^+) (step a_1/b_1), and may use the invariant Ser57−nucleotide N3 interaction to deter protonation at N3. Kinetic studies show that *Aa*PurE is inhibited by a protonation (pK_1) that is relatively insensitive to the His59 → Asp mutation. We therefore assign pK_1 to protonation of CAIR N3, which would give a dead end species (labeled pK_1 in Figure 8). Because the interaction with Ser57 is affected, N3-protonated CAIR might be bound in an unproductive configuration that would allow only the decarboxylation half-reaction. This low-pH route for the conversion of CAIR → AIR, without intermediate formation of N^5-CAIR, may explain why AIR is observed in several

Scheme 2

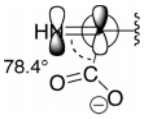

*Aa*PurE·AIR complexes characterized at low pH. AIR·*Aa*PurE complexes may even serve to inhibit purine biosynthesis at low pH.

IsoCAIR Is a Plausible On-Pathway Intermediate. Protonation of CAIR C4 during the PurE reaction was expected to occur (*5*, *51*) because of the acid-mediated decarboxylation of CAIR and analogues (*33*). The readily exchangeable AIR H4 (*5*) also provides some precedent for transient formation and protonation of a C4 carbanion. Indeed, the C4-methylene, C5-imino tautomer of AIR is believed to be a late intermediate in the AIR synthetase (PurM) reaction (*19*, *52*).

The decarboxylation of 2-substituted benzoic acid derivatives, a possible model for CAIR decarboxylation, is thought to be a multistep process: protonation of the carbon α to the carboxylate to form an sp^3-hybrized intermediate and then decarboxylation of this protonated intermediate. For anthranilic acid, decarboxylation becomes rate limiting at low pH and more fully rate limiting in 10 M H_2SO_4 ($^{12}C/^{13}C$ carbonyl kinetic isotope effect, KIE, of 3.7%) (*53*, *54*). In strong acid, decarboxylation is hampered by the poor leaving group ability of CO_2H^+. Acid catalysis and a 1.8% ^{13}C KIE are observed in 2,4-dihydroxybenzoic acid at pH 5.3, where the carboxylate is predominantly ionized (*55*). Stereoelectronic considerations suggest that decarboxylation is facilitated when the carboxylate C−Cα bond is perpendicular to the *β*-iminium or protonated ketone.

Why Is the isoCAIR Carboxylate C−C4 Bond Intact in Crystal Structure 2fwp? H59N-*Aa*PurE accumulates isoCAIR because it stabilizes this otherwise unlikely (protonated) CAIR tautomer but is unable to trigger C−C bond scission. Stabilization is evident from the large number of hydrogen-bonding interactions between isoCAIR and PurE, which outnumber the interactions between AIR and PurE (Figure S5 in Supporting Information). Neither proton transfer nor geometric constraints seem to prevent isoCAIR(·H^+) decarboxylation when bound to H59N-*Aa*PurE. In the 2fwp structure, isoCAIR shows a nearly ideal torsion angle of 78.4° between substituents (Scheme 2). The isoCAIR substituents share a bound water (HOH165), which is positioned to serve as a proton shuttle; it may even be a hydroxide ion, stabilized by three interactions with backbone NHs. If PurE uses mechanism a, initial carboxylate C−C4 scission (step b_2) is circumvented by rapid deprotonation of the exocyclic iminium, using His59 or water 165 as the base. (Equivalently, the isoCAIR carboxylate might be protonated to prevent decarboxylation.) The use of His59 to deprotonate the exocyclic iminium makes the most sense because step a_3 would be difficult without a protonated residue available to stabilize the azaenolate intermediate. Hence the H59N-*Aa*PurE mutant would be unable to perform this step, leading to the observed accumulation of isoCAIR. In contrast, if *Aa*PurE uses mechanism b, there is no obvious reason why the His59 → Asn substitution would be unable to perform step b_2 (i.e., C−C bond scission would have been observed). For this reason, we favor mechanism a although some features of mechanism b remain plausible and are discussed below.

Scheme 3

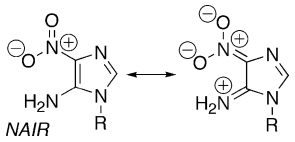

An alternative to our working mechanism would be concerted C−C bond scission and protonation of the nascent carbanion by His59, producing trapped AIR and CO_2 in the active site. A similar mechanism was proposed for the challenging decarboxylation performed by orotidine 5′-monophosphate decarboxylase, where the acid is a protonated Lys and the nucleotide substrate, like isoCAIR, is bound tightly by the enzyme (*56*, *57*). General acid catalysts have been shown to affect the nonenzymatic decarboxylation of mandelylthiamin by trapping the carbanion with a proton, which accelerates the dissociation of a "sticky" CO_2 (*58*). The dissociated CO_2 then reacts with a different carbanion. In the alternative mechanism, the internal "recarboxylation" half-reaction that is unique to PurE would be performed by the less reactive species AIR and CO_2 and would require concomitant deprotonation of AIR. This alternative would easily unite the class I and class II PurE mechanisms. However, our simpler working hypothesis, in which protonated His59 facilitates C−C scission (step a_3) without irreversibly quenching the carbanion (step b_{-3}), requires fewer proton transfers and a reactive carbanionic intermediate that is not accessible to most His59 mutants. As a limiting explanation for why active *Aa*PurE requires an ionizable residue at position 59, reversible proton transfer to the azaenolate (steps b_3/b_{-3}) might be in a rapid equilibrium that terminates with nucleophilic attack by the azaenolate on trapped CO_2.

Mechanistic Divergence in PurE Classes. Class II PurE is believed to consume a proton in the reverse direction (CAIR → AIR, Scheme 1), and its K_i for 4-nitro-AIR (NAIR) is substantially lower (0.34 nM for *Gallus gallus* PurE versus 0.5 μM for *Ec*PurE) (*6*, *51*)). The class I $K_{i,NAIR}$ is very similar to the values reported here for $K_{d,CAIR}$ and H89G-*Aa*PurE $K_{m,CAIR}$, indicating NAIR is mainly a CAIR analogue for class I PurEs. Unlike CAIR, NAIR is not a Brønsted acid or base in a biologically significant range: the analogue 1,2-dimethyl-4-nitro-5-aminoimidazole has $pK_a = 0.33$ (*59*). NAIR has partial positive character on the exocylic amino group and C5, like the isoCAIR·H^+ zwitterion, but it also has partial double bond character between the nitro N and C4, which keeps the nitro group in the plane of the imidazole ring (Scheme 3). The highly nonplanar isoCAIR geometry observed here is quite different. The high-affinity class II PurE−NAIR interaction, which perturbs the electronic structure of NAIR (*51*), suggests that NAIR resembles a transition state that is not used by class I PurEs. One candidate is a planar intermediate formed prior to proton transfer to CAIR C4 (*51*), with a C replacing the NAIR nitro N^+ in the right resonance structure in Scheme 3.

ACKNOWLEDGMENT

T.J.K. thanks JoAnne Stubbe for introducing him to PurE. We thank Kevin Moeller and JoAnne Stubbe for comments

on the manuscript. We thank Jake Schaefer, Dewey Holten, and Chris Kirmaier for the use of equipment. We thank Zhiwei Chen and F. Scott Mathews for help with X-ray data collection.

SUPPORTING INFORMATION AVAILABLE

Partial purification of *Aa*PurK, isolation of H6*Aa*PurK, and gel comparison (Figure S1); determination of extinction coefficients for the reverse-reaction activity assay at other pH values (Figure S2); tables of ODNs, carboxylate-*Aa*PurE K_ds, and additional crystallographic data and refinement statistics; views of two active sites showing possible proton tunnels and bound ligands, as stereo diagrams or simple images (Figures S3 and S4); a LigPlot rendering of the isoCAIR-bound active site in structure 2fwp (Figure S5). This material is available free of charge via the Internet at http://pubs.acs.org.

REFERENCES

1. Kappock, T. J., Ealick, S. E., and Stubbe, J. (2000) Modular evolution of the purine biosynthetic pathway, *Curr. Opin. Chem. Biol. 4*, 567−572.
2. Mathews, I. I., Kappock, T. J., Stubbe, J., and Ealick, S. E. (1999) Crystal structure of *Escherichia coli* PurE, an unusual mutase in the purine biosynthetic pathway, *Structure 7*, 1395−1406.
3. Mueller, E. J., Meyer, E., Rudolph, J., Davisson, V. J., and Stubbe, J. (1994) N^5-carboxyaminoimidazole ribonucleotide: Evidence for a new intermediate and two new enzymatic activities in the *de novo* purine biosynthetic pathway of *Escherichia coli*, *Biochemistry 33*, 2269−2278.
4. Meyer, E., Leonard, N. J., Bhat, B., Stubbe, J., and Smith, J. M. (1992) Purification and characterization of the *pur*E, *pur*K, and *pur*C gene products: identification of a previously unrecognized energy requirement in the purine biosynthetic pathway, *Biochemistry 31*, 5022−5032.
5. Meyer, E., Kappock, T. J., Osuji, C., and Stubbe, J. (1999) Evidence for the direct transfer of the carboxylate of N^5-carboxyaminoimidazole ribonucleotide (N^5-CAIR) to generate 4-carboxy-5-aminoimidazole ribonucleotide catalyzed by *Escherichia coli* PurE, an N^5-CAIR mutase, *Biochemistry 38*, 3012−3018.
6. Firestine, S. M., Poon, S.-W., Mueller, E. J., Stubbe, J., and Davisson, V. J. (1994) Reactions catalyzed by 5-aminoimidazole ribonucleotide carboxylases from *Escherichia coli* and *Gallus gallus*: a case for divergent catalytic mechanisms, *Biochemistry 33*, 11927−11934.
7. Waldrop, G. L., Rayment, I., and Holden, H. M. (1994) Three-dimensional structure of the biotin carboxylase subunit of acetyl-CoA carboxylase, *Biochemistry 33*, 10249−10256.
8. Thoden, J. B., Kappock, T. J., Stubbe, J., and Holden, H. M. (1999) Three-dimensional structure of N^5-carboxyaminoimidazole ribonucleotide synthetase: A member of the ATP grasp protein superfamily, *Biochemistry 38*, 15480−15492.
9. Kluger, R., and Adawadkar, P. D. (1976) A reaction proceeding through intramolecular phosphorylation of a urea. A chemical mechanism for enzymatic carboxylation of biotin involving cleavage of ATP, *J. Am. Chem. Soc. 98*, 3741−3742.
10. Ogita, T., and Knowles, J. R. (1988) On the intermediacy of carboxyphosphate in biotin-dependent carboxylations, *Biochemistry 27*, 8028−8033.
11. Asai, T. (1968) *Acetic acid bacteria. Classification and biochemical activities*, University of Tokyo Press, Tokyo.
12. Menzel, U., and Gottschalk, G. (1985) The internal pH of *Acetobacterium wieringae* and *Acetobacter aceti* during growth and production of acetic acid, *Arch. Microbiol. 143*, 47−51.
13. Settembre, E. C., Chittuluru, J. R., Mill, C. P., Kappock, T. J., and Ealick, S. E. (2004) Acidophilic adaptations in the structure of *Acetobacter aceti* N^5-carboxyaminoimidazole ribonucleotide mutase (PurE), *Acta Crystallogr., Sect. D: Biol. Crystallogr. D60*, 1753−1760.
14. Schendel, F. J. (1986) Ph.D. Thesis, University of Wisconsin, Madison, WI.
15. Firestine, S. M., and Davisson, V. J. (1994) Carboxylases in de novo purine biosynthesis. Characterization of the *Gallus gallus* bifunctional enzyme, *Biochemistry 33*, 11917−11926.
16. Srivastava, P. C., Mancuso, R. W., Rousseau, R. J., and Robins, R. K. (1974) Nucleoside peptides. 6. Synthesis of certain N-(5-amino-1-(β-D-ribofuranosyl)imidazole-4-carbonyl)amino acids related to naturally occurring intermediates in the purine biosynthetic pathway, *J. Med. Chem. 17*, 1207−1211.
17. Stouthamer, A. H., de Haan, P. G., and Nijkamp, H. J. (1965) Mapping of purine markers in *Escherichia coli* K 12, *Genet. Res. 6*, 442−453.
18. Staden, R., Beal, K. F., and Bonfield, J. K. (2000) The Staden package, 1998, *Methods Mol. Biol. 132*, 115−130.
19. Schrimsher, J. L., Schendel, F. J., and Stubbe, J. (1986) Isolation of a multifunctional protein with aminoimidazole ribonucleotide synthetase, glycinamide ribonucleotide synthetase, and glycinamide ribonucleotide transformylase activities: Characterization of aminoimidazole ribonucleotide synthetase, *Biochemistry 25*, 4356−4365.
20. Ellis, K. J., and Morrison, J. F. (1982) Buffers of constant ionic strength for studying pH-dependent processes, *Methods Enzymol. 87*, 405−426.
21. Bates, R. G., and Pinching, G. D. (1949) Resolution of the dissociation constants of citric acid at 0 to 50, and determination of certain related thermodynamic functions, *J. Am. Chem. Soc. 71*, 1274−1283.
22. Brünger, A. T., Adams, P. D., Clore, G. M., DeLano, W. L., Gros, P., Grosse-Kunstleve, R. W., Jiang, J.-S., Kuszewski, J., Nilges, M., Pannu, N. S., Read, R. J., Rice, L. M., Simonson, T., and Warren, G. L. (1998) Crystallography & NMR system: A new software suite for macromolecular structure determination, *Acta Crystallogr., Sect. D: Biol. Crystallogr. D54*, 905−921.
23. Jones, T. A., Zou, J. Y., Cowan, S. W., and Kjeldgaard (1991) Improved methods for building protein models in electron density maps and the location of errors in these models, *Acta Crystallogr. A 47*, 110−119.
24. Kleywegt, G. J., and Jones, T. A. (1998) Databases in protein crystallography, *Acta Crystallogr., Sect. D: Biol. Crystallogr. 54*, 1119−1131.
25. Schüttelkopf, A. W., and van Aalten, D. M. F. (2004) PRODRG: a tool for high-throughput crystallography of protein−ligand complexes, *Acta Crystallogr., Sect. D: Biol. Crystallogr. 60*, 1355−1363.
26. Vagin, A. A., Steiner, R. A., Lebedev, A. A., Potterton, L., McNicholas, S., Long, F., and Murshudov, G. N. (2004) REFMAC5 dictionary: organization of prior chemical knowledge and guidelines for its use, *Acta Crystallogr., Sect. D: Biol. Crystallogr. 60*, 2184−2195.
27. Collaborative Computational Project No. 4 (1994) The CCP4 suite: programs for protein crystallography, *Acta Crystallogr. D 50*, 760−770.
28. Kraulis, P. J. (1991) Molscript: A program to produce both detailed and schematic plots of protein structures, *J. Appl. Crystallogr. 24*, 946−950.
29. Merritt, E. A., and Bacon, D. J. (1997) Raster3D: Photorealistic molecular graphics, *Methods Enzymol. 277*, 505−524.
30. DeLano, W. L. (2002) *The PyMOL Users Manual*, San Carlos, CA.
31. Meyer, E. (1996), Ph.D. Thesis, Massachusetts Institute of Technology, Cambridge, MA.
32. Bernal, J. D., and Fowler, R. H. (1933) A theory of water and ionic solution, with particular reference to hydrogen and hydroxyl ions, *J. Chem. Phys. 1*, 515−548.
33. Litchfield, G. J., and Shaw, G. (1971) Purines, pyrimidines, and imidazoles. Part XXXVIII. A kinetic study of the decarboxylation of 5-amino-1-β-D-ribofuranosylimidazole-4-carboxylic acid 5′-phosphate and related compounds, *J. Chem. Soc. B*, 1474−1484.
34. Smithers, G. W., and O'Sullivan, W. J. (1982) ^{31}P nuclear magnetic resonance study of phosphoribosyldiphosphate and its interaction with magnesium ions, *J. Biol. Chem. 257*, 6164−6170.
35. Boyle, M. P., Kalliomaa, A. K., Levdikov, V., Blagova, E., Fogg, M. J., Brannigan, J. A., Wilson, K. S., and Wilkinson, A. J. (2005) Crystal structure of PurE (BA0288) from *Bacillus anthracis* at 1.8 Å resolution, *Proteins 61*, 674−676.
36. Loladze, V. V., Ibarra-Molero, B., Sanchez-Ruiz, J. M., and Makhatadze, G. I. (1999) Engineering a thermostable protein via optimization of charge−charge interactions on the protein surface, *Biochemistry 38*, 16419−16423.

37. Schwehm, J. M., Fitch, C. A., Dang, B. N., Garcia-Moreno, E. B., and Stites, W. E. (2003) Changes in stability upon charge reversal and neutralization substitution in staphylococcal nuclease are dominated by favorable electrostatic effects, *Biochemistry 42*, 1118−1128.
38. Spector, S., Wang, M., Carp, S. A., Robblee, J., Hendsch, Z. S., Fairman, R., Tidor, B., and Raleigh, D. P. (2000) Rational modification of protein stability by the mutation of charged surface residues, *Biochemistry 39*, 872−879.
39. Strickler, S. S., Gribenko, A. V., Keiffer, T. R., Tomlinson, J., Reihle, T., Loladze, V. V., and Makhatadze, G. I. (2006) Protein stability and surface electrostatics: a charged relationship, *Biochemistry 45*, 2761−2766.
40. Koide, A., Jordan, M. R., Horner, S. R., Batori, V., and Koide, S. (2001) Stabilization of a fibronectin type III domain by the removal of unfavorable electrostatic interactions on the protein surface, *Biochemistry 40*, 10326−10333.
41. Makhatadze, G. I., Loladze, V. V., Ermolenko, D. N., Chen, X., and Thomas, S. T. (2003) Contribution of surface salt bridges to protein stability: guidelines for protein engineering, *J. Mol. Biol. 327*, 1135−1148.
42. Hendsch, Z. S., and Tidor, B. (1994) Do salt bridges stabilize proteins? A continuum electrostatic analysis, *Protein Sci. 3*, 211−226.
43. Steiner, H., Jonsson, B. H., and Lindskog, S. (1975) The catalytic mechanism of carbonic anhydrase. Hydrogen-isotope effects on the kinetic parameters of the human C isoenzyme, *Eur. J. Biochem. 59*.
44. Silverman, D. N., and Lindskog, S. (1988) The catalytic mechanism of carbonic anhydrase: Implications of a rate-limiting protolysis of water, *Acc. Chem. Res. 21*, 30−36.
45. Frank, R. A. W., Titman, C. M., Pratap, J. V., Luisi, B. F., and Perham, R. N. (2004) A molecular switch and proton wire synchronize the active sites in thiamine enzymes, *Science 306*, 872−876.
46. Babbitt, P. C., Hasson, M. S., Wedekind, J. E., Palmer, D. R., Barrett, W. C., Reed, G. H., Rayment, I., Ringe, D., Kenyon, G. L., and Gerlt, J. A. (1996) The enolase superfamily: a general strategy for enzyme-catalyzed abstraction of the α-protons of carboxylic acids, *Biochemistry 35*, 16489−16501.
47. Gerlt, J. A., Babbitt, P. C., and Rayment, I. (2005) Divergent evolution in the enolase superfamily: the interplay of mechanism and specificity, *Arch. Biochem. Biophys. 433*, 59−70.
48. Fersht, A. (2000) *Structure and mechanism in protein science*, W. H. Freeman and Co., New York.
49. Litchfield, G. J., and Shaw, G. (1965) The mechanism of decarboxylation of some 5-aminoimidazole-4-carboxylic acids and the influence of transition metals, *Chem. Commun.*, 563−565.
50. Litchfield, G. J., and Shaw, G. (1971) Purines, pyrimidines, and imidazoles. Part XXXV. Potentiometric and spectroscopic studies of some imidazoles related to intermediates in the biosynthesis *de novo* of purine nucleotides, *J. Chem. Soc. C*, 817−820.
51. Firestine, S. M., and Davisson, V. J. (1993) A tight binding inhibitor of 5-aminoimidazole ribonucleotide carboxylase, *J. Med. Chem. 36*, 3484−3486.
52. Schrimsher, J. L., Schendel, F. J., Stubbe, J., and Smith, J. M. (1986) Purification and characterization of aminoimidazole ribonucleotide synthetase from *Escherichia coli*, *Biochemistry 25*, 4366−4371.
53. Dunn, G. E., and Dayal, S. K. (1970) Mechanism of decarboxylation of substituted anthranilic acids at high acidity, *Can. J. Chem. 48*, 3349−3353.
54. Willi, A. V., Won, C. M., and Vilk, P. (1968) Kinetics and mechanism of the decarboxylation of anthranilic acid in aqueous solution, *J. Phys. Chem. 72*, 3142−3148.
55. Lynn, K. R., and Bourns, A. N. (1963) ^{13}Carbon kinetic isotope effects and the mechanism of decarboxylation of 2,4-dihydroxybenzoic acid, *Chem. Ind.*, 782−783.
56. Appleby, T. C., Kinsland, C., Begley, T. P., and Ealick, S. E. (2000) The crystal structure and mechanism of orotidine 5′-monophosphate decarboxylase, *Proc. Natl. Acad. Sci. U.S.A. 97*, 2005−2010.
57. Begley, T. P., Appleby, T. C., and Ealick, S. E. (2000) The structural basis for the remarkable catalytic proficiency of orotidine 5′-monophosphate decarboxylase, *Curr. Opin. Struct. Biol. 10*, 711−718.
58. Hu, Q., and Kluger, R. (2005) Making thiamin work faster: acid-promoted separation of carbon dioxide, *J. Am. Chem. Soc. 127*, 12242−12243.
59. Blazevic, N., Kajfez, F., and Sunjic, V. (1970) σ values of some nitroimidazoles, *J. Heterocycl. Chem. 7*, 227−229.
60. Hodel, A., Kim, S. H., and Brünger, A. T. (1992) Model bias in macromolecular crystal structures, *Acta Crystallogr. A 48*, 851−858.
61. Francois, J. A., and Kappock, T. J. (2006) Alanine racemase from the acidophile *Acetobacter aceti*, *Protein Expression Purif.* (in press).
62. Chan, J. W., and Goodwin, P. H. (1995) Extraction of genomic DNA from extracellular polysaccharide-synthesizing Gram-negative bacteria, *BioTechniques 18*, 418−422.

BI060465N